Electronic Supplementary Information

Controlling Enzyme Reactions by Supramolecular Protection and Deprotection of Oligosaccharide Substrates

Milad Zangiabadi and Yan Zhao*
Department of Chemistry, Iowa State University, Ames, Iowa 50011-3111, USA
**E-mail: zhaoy@iastate.edu*

Table of Contents

General Method

All organic solvents and reagents were of ACS-certified grade or higher grade, and were purchased from commercial suppliers. Maltase enzyme was purchased from Megazyme (Product code E-MALTS). MBAm was purchased from Affymetrix Inc. The glucose assay kit was purchased from Sigma (SKU # GAHK20). Milli-Q water (18.2 MU; Millipore Co., USA) was used for MINP preparation and all the buffers. Routine ^{1}H and ^{13}C NMR spectra were recorded on a Bruker DRX-400 or a Varian VXR-400 NMR spectrometer. ESI-MS mass was recorded on Shimadzu LCMS-2010 mass spectrometer. Dynamic light scattering (DLS) data were recorded at 25 °C on a Malvern Zetasizer Nano ZS analyzer. Isothermal titration calorimetry (ITC) was performed using a MicroCal VP-ITC Microcalorimeter with Origin 7 software and VPViewer2000 (GE Healthcare, Northampton, MA). Transmission electron microscopy (TEM) was performed on a 200kV JEOL 2100 scanning/transmission electron microscope with <1.4 Å resolution and integrated software package for computerized control. UV-vis spectra were recorded on a Cary 100 Bio UV-visible spectrophotometer. LC-MS analysis was performed with a Thermo Scientific HILIC-LC column (4.6 mm, 150 mm) coupled to an Agilent 1200 Series Binary VWD system with an Agilent 6540 UHD Accurate Mass Q-TOF mass spectrometry detector.

Syntheses

Syntheses of compounds **1**,[1] **2**,[2] **3**,[1] **13**,[2] 4-nitrobenzohydrazide,[3] adamantane-1-carbohydrazide,[4] octanohydrazide,[5] hexanohydrazide,[6] decanohydrazide,[7] and dodecanohydrazide [8] were previously reported.

General procedure for the synthesis of templates (4a–4d, 11, 12 and 15)
Templates were synthesized following a modified literature procedure.[9] To a solution of the appropriate oligosaccharide (3.0 mmol) in methanol (6 mL) was added the acyl hydrazide (3.0 mmol) and aniline as the catalyst (0.006 mmol). The reaction mixture was heated to reflux overnight under N_2. After it was cooled to room temperature, solvent was removed by rotary evaporation. The residue was purified by column chromatography over silica gel using 2:1 dichloromethane/methanol as the eluent. The resulting solids then were poured in diethyl ether to remove residual nonpolar impurities, filtered and dried under vacuum to afford the final product.

Compound (4a). Yellow powder (1.25 g, 83% yield, 12 : 88 mixture of α/β anomers). ^{1}H NMR (400 MHz, D_2O, δ): 8.15 (d, *J* = 8.8 Hz, 2H), 7.75 (d, *J* = 8.8 Hz, 2H), 5.23 (d, *J* = 4.0 Hz, 1H), 4.47 (d, *J* = 8.0 Hz, 0.12H$_\alpha$), 4.08 (d, *J* = 9.2 Hz, 0.88H$_\beta$), 3.36-3.76 (m, 10H), 3.21-3.27 (m, 2H). ^{13}C NMR (100 MHz, D_2O, δ): 168.5, 149.6, 138.1, 128.6, 123.8, 99.6, 89.7, 76.7, 75.5, 72.8, 72.6, 71.6, 70.6, 69.3, 60.8, 60.4, 48.8 ppm. ESI-QTOF-HRMS (m/z): $[M + H]^+$ calcd for $C_{19}H_{27}N_3O_{13}$ 506.1577; found, 506.1622.

Compound (4b). White powder (1.21 g, 78% yield, 20 : 80 mixture of α/β anomers). ^{1}H NMR (400 MHz, D_2O, δ): 5.30 (d, *J* = 4.0 Hz, 1H), 4.50 (d, *J* = 5.2 Hz, 0.20H$_\alpha$), 3.99 (d, *J* = 9.2 Hz, 0.80H$_\beta$), 3.47-3.76 (m, 10H), 3.33 (t, *J* = 9.6 Hz, 1H), 3.21 (t, *J* = 9.6 Hz, 1H), 1.93-1.95 (m, 3H), 1.75-1.77 (m, 6H), 1.60-1.70 (m, 6H). ^{13}C NMR (100 MHz, D_2O, δ): 189.9, 99.7, 89.9, 87.6, 77.0, 76.6, 75.5, 73.3,

---

[1] Awino, J. K.; Zhao, Y. Protein-Mimetic, Molecularly Imprinted Nanoparticles for Selective Binding of Bile Salt Derivatives in Water. *J. Am. Chem. Soc*. **2013**, 135, 12552-12555.
[2] Gunasekara, W. R.; Zhao, Y. A General Method for Selective Recognition of Monosaccharides and Oligosaccharides in Water. *J. Am. Chem. Soc*. **2017**, 139, 829-835.
[3] Rodrigues, D. A.; Guerra, F. S.; Sagrillo, F. S.; de Sena M Pinheiro, P.; Alves, M. A.; Thota, S.; Chaves, L. S.; Sant'Anna, C. M. R.; Fernandes, P. D.; Fraga, C. A. M. Design, Synthesis, and Pharmacological Evaluation of First-in-Class Multitarget N-Acylhydrazone Derivatives as Selective HDAC6/8 and PI3Kα Inhibitors. *ChemMedChem* **2020**, 15 (6), 539–551
[4] Luo, G.-F.; Xu, X.-D.; Zhang, J.; Yang, J.; Gong, Y.-H.; Lei, Q.; Jia, H.-Z.; Li, C.; Zhuo, R.-X.; Zhang, X.-Z. Encapsulation of an Adamantane-Doxorubicin Prodrug in PH-Responsive Polysaccharide Capsules for Controlled Release. *ACS Appl. Mater. Interfaces* **2012**, 4 (10), 5317–5324.
[5] Palace-Berl, F.; Pasqualoto, K. F. M.; Jorge, S. D.; Zingales, B.; Zorzi, R. R.; Silva, M. N.; Ferreira, A. K.; de Azevedo, R. A.; Teixeira, S. F.; Tavares, L. C. Designing and Exploring Active N'-[(5-Nitrofuran-2-Yl) Methylene] Substituted Hydrazides against Three Trypanosoma Cruzi Strains More Prevalent in Chagas Disease Patients. *Eur. J. Med. Chem*. **2015**, 96, 330–339.
[6] Fulton, D. A. Dynamic Combinatorial Libraries Constructed on Polymer Scaffolds. *Org. Lett*. **2008**, 10 (15), 3291–3294.
[7] Meyer, F.; Ueberschaar, N.; Hertweck, C. Concise Total Synthesis of Hydrazidomycin A, a Rare Hydrazide Metabolite of Streptomyces Atratus. *Europ. J. of Org. Chem* **2013**, 20, 4242–4244.
[8] Smith, M. M.; Edwards, W.; Smith, D. K. Self-Organisation Effects in Dynamic Nanoscale Gels Self-Assembled from Simple Mixtures of Commercially Available Molecular-Scale Components. *Chem. Sci.* **2013**, 4 (2), 671–676.
[9] Coxon, T.P.; Fallows, T.W.; Gough, J.E.; Webb, S.J. A versatile approach towards multivalent saccharide displays on magnetic nanoparticles and phospholipid vesicles. *Chem. Comm.* **2015**, 13, 10751-10761.

72.9, 72.8, 72.6, 71.6, 70.4, 70.2, 69.3, 60.7, 60.4, 48.8, 40.0, 38.3, 38.2, 35.7, 27.6 ppm. ESI-QTOF-HRMS (m/z): $[M + H]^+$ calcd for $C_{22}H_{36}N_2O_{11}$ 519.2509; found, 519.2561.

Compound (4c, n = 7**).** White powder (1.28 g, 89% yield, 15 : 85 mixture of α/β anomers). ^{1}H NMR (400 MHz, D_2O, δ): 5.20 (d, J = 4.0 Hz, 1H), 4.47 (d, J = 4.8 Hz, 0.15H_α), 3.91 (d, J = 9.2 Hz, 0.85H_β), 3.35-3.76 (m, 11H), 3.25 (t, J = 9.2 Hz, 1H), 2.06 (t, J = 7.2 Hz, 2H), 1.11-1.13 (m, 8H), 0.70 (t, J = 6.8 Hz, 3H). ^{13}C NMR (100 MHz, D_2O, δ): 176.3, 99.7, 89.6, 77.1, 76.6, 75.6, 72.8, 72.7, 71.7, 70.5, 69.2, 60.8, 60.4, 33.7, 31.1, 30.2, 28.1, 25.1, 22.0, 13.4 ppm. ESI-QTOF-HRMS (m/z): $[M + H]^+$ calcd for $C_{20}H_{38}N_2O_{11}$ 483.2509; found, 483.2555.

Compound (4c, n = 5**).** White powder (1.27 g, 93% yield, 10 : 90 mixture of α/β anomers). ^{1}H NMR (400 MHz, D_2O, δ): 5.21 (d, J = 3.6 Hz, 1H), 4.47 (d, J = 4.4 Hz, 0.10H_α), 3.91 (d, J = 9.2 Hz, 0.90H_β), 3.35-3.75 (m, 11H), 2.23 (t, J = 9.2 Hz, 1H), 2.05 (t, J = 7.2 Hz, 2H), 1.39-1.46 (m, 2H), 1.05-1.18 (m, 4H), 0.69 (t, J = 9.2 Hz, 3H). ^{13}C NMR (100 MHz, D_2O, δ): 176.5, 99.6, 89.6, 76.9, 76.7, 75.5, 72.8, 72.7, 71.6, 70.5, 69.3, 60.9, 60.4, 33.7, 30.3, 24.8, 21.6, 13.2 ppm. ESI-QTOF-HRMS (m/z): $[M + H]^+$ calcd for $C_{18}H_{34}N_2O_{11}$ 455.2196; found, 455.2245.

Compound (4c, n = 9**).** White powder (1.31 g, 85% yield, 10 : 90 mixture of α/β anomers). ^{1}H NMR (400 MHz, D_2O, δ): 5.26 (d, J = 4.4 Hz, 1H), 4.53 (d, J = 3.2 Hz, 0.10H_α), 3.99 (d, J = 8.8 Hz, 0.90H_β), 3.34-3.84 (m, 12H), 2.10-2.20 (m, 2H), 1.47-1.58 (m, 2H), 1.10-1.34 (m, 12H), 0.73-0.85 (m, 3H). ^{13}C NMR (100 MHz, D_2O, δ): 175.9, 99.5, 89.9, 77.1, 77.0, 75.3, 72.8, 72.6, 71.6, 70.7, 69.3, 60.9, 60.4, 48.2, 48.0, 31.3, 28.9, 28.7, 28.3, 25.2, 22.2, 13.5 ppm. ESI-QTOF-HRMS (m/z): $[M + H]^+$ calcd for $C_{22}H_{42}N_2O_{11}$ 511.2822; found, 511.2879.

Compound (4c, n = 11**).** White powder (1.38 g, 86% yield, less than 5% mixture of α/β anomers). ^{1}H NMR (400 MHz, D_2O, δ): 5.26 (br, 1H), 3.99 (br, 1H$_\beta$), 3.27-3.83 (m, 12H), 2.05-2.23 (m, 2H), 1.45-1.62 (m, 2H), 1.07-1.34 (m, 16H), 0.70-0.87 (m, 3H). ^{13}C NMR (100 MHz, D_2O, δ): 174.7, 100.4, 90.2, 78.0, 76.6, 75.7, 73.0, 72.8, 71.8, 70.7, 69.2, 60.8, 60.5, 48.8, 34.0, 32.0, 30.1, 30.0, 29.7, 29.6, 29.5, 25.6, 22.7, 13.8 ppm. ESI-QTOF-HRMS (m/z): $[M + H]^+$ calcd for $C_{24}H_{46}N_2O_{11}$ 539.3135; found, 539.3191.

Compound (4d). White powder (1.33 g, 76% yield, less than 5% mixture of α/β anomers). ^{1}H NMR (400 MHz, DMSO-*d*$_6$, δ): 8.45-8.48 (m, 1H), 8.31-8.36 (m, 3H), 8.20-8.28 (m, 3H), 8.09-8.13 (m, 2H), 5.03 (d, J = 4.0 Hz, 1H), 4.09 (d, J = 9.2 Hz, 1H$_\beta$), 3.45-3.75 (m, 9H), 3.18-3.26 (m, 2H), 3.00-3.09 (m, 1H). ^{13}C NMR (100 MHz, DMSO-d_6, δ): 168.5, 132.3, 131.1, 130.6, 128.9, 128.8, 128.5, 127.6, 127.1, 126.4, 126.1, 126.0, 124.9, 124.8, 124.1, 124.0, 101.3, 91.1, 80.5, 76.8, 76.6, 73.9, 72.7, 71.3, 70.2, 61.4, 61.1, 48.9, 45.3 ppm. ESI-QTOF-HRMS (m/z): $[M + H]^+$ calcd for $C_{29}H_{32}N_2O_{11}$ 585.2040; found, 585.2077.

Compound (11). White powder (1.25 g, 87% yield, 13 : 87 mixture of α/β anomers). ^{1}H NMR (400 MHz, D_2O, δ): 4.45 (d, J = 4.8 Hz, 0.13H_α), 4.24 (d, J = 7.6 Hz, 0.87H), 3.90 (d, J = 9.2 Hz, 1H$_\beta$), 3.31-3.83 (m, 10H), 3.14 (t, J = 8.0 Hz, 1H), 2.01-2.08 (m, 2H), 1.41-1.45 (m, 2H), 1.04-1.22 (m, 8H), 0.66-0.76 (m, 3H). ^{13}C NMR (100 MHz, D_2O, δ): 176.3, 99.7, 89.6, 77.1, 76.7, 75.6, 72.8, 72.7, 71.7, 70.5, 70.1, 69.2, 60.8, 60.4, 33.7, 31.1, 30.2, 28.1, 25.1, 22.0, 13.4 ppm. ESI-QTOF-HRMS (m/z): $[M + H]^+$ calcd for $C_{20}H_{38}N_2O_{11}$ 483.2509; found, 483.2570.

Compound (12). White powder (1.59 g, 82% yield, 12 : 88 mixture of α/β anomers). ^{1}H NMR (400 MHz, D_2O, δ): 5.31 (d, J = 4.0 Hz, 1H), 5.30 (d, J =4.0 Hz, 1H), 4.56 (d, J = 5.2 Hz, 0.12H$_\alpha$), 4.01 (d, J = 9.2 Hz, 0.88H$_\beta$), 3.47-3.89 (m, 16H), 3.34 (t, J = 9.2 Hz, 1H), 3.24 (t, J = 9.2 Hz, 1H), 2.16 (t, J = 7.2 Hz, 2H), 1.46-1.58 (m, 2H), 1.14-1.29 (m, 8H), 0.79 (t, J = 7.2 Hz, 3H). ^{13}C NMR (100 MHz, D_2O, δ): 176.5, 99.7, 99.6, 89.6, 77.1, 76.7, 76.6, 75.5, 73.3, 72.8, 72.6, 71.7, 71.4, 71.1, 70.4, 69.3, 66.0, 60.7, 60.4, 33.6, 30.9, 28.0, 27.9, 25.1, 21.9, 14.0, 13.4 ppm. ESI-QTOF-HRMS (m/z): $[M + H]^+$ calcd for $C_{26}H_{48}N_2O_{16}$ 645.3037; found, 645.3092.

Compound (15). White powder (1.00 g, 79% yield, less than 5% mixture of α/β anomers). ^{1}H NMR (400 MHz, DMSO-d_6, δ): 8.45-8.49 (m, 1H), 8.31-8.36 (m, 3H), 8.20-8.27 (m, 3H), 8.09-8.13 (m, 2H), 4.04 (d, J = 9.2 Hz, 1H$_\beta$), 3.45-3.73 (m, 3H), 3.44 (m, 2H), 3.28 (t, J = 8.8 Hz,1H), 3.14 (t, J = 8.8 Hz,1H), 3.07 (t, J = 9.2 Hz,1H). ^{13}C NMR (100 MHz, DMSO-d_6, δ): 168.4, 132.2, 131.1, 130.6, 130.2, 128.9, 128.7, 128.5, 127.6, 127.1, 126.3, 126.1, 126.0, 124.9, 124.8, 124.1, 124.0, 91.2, 78.4, 77.0, 71.8, 70.7, 61.8 ppm. ESI-QTOF-HRMS (m/z): $[M + H]^+$ calcd for $C_{23}H_{22}N_2O_6$ 423.1511; found, 423.1535.

Preparation of MINP

A typical procedure is as follows. To a micellar solution of compound **1** (0.03 mmol) and compound **2** (0.02 mmol) in H_2O (2.0 mL), divinylbenzene (DVB, 2.8 μL, 0.02 mmol), MBAm (0.02 mmol), the appropriate template (**4a**–**4d**) in H_2O (10 μL of a solution of 0.04 mmol/mL, 0.0004 mmol), and 2,2-dimethoxy-2-phenylacetophenone (DMPA,10 μL of a 12.8 mg/mL solution in DMSO, 0.0005 mmol) were added. The mixture was subjected to ultrasonication for 10 min before $CuCl_2$ (10 μL of a 6.7 mg/mL solution in H_2O, 0.0005 mmol), and sodium ascorbate (10 μL of a 99 mg/mL solution in H_2O, 0.005 mmol) were added. After the reaction mixture was stirred slowly at room temperature for 12 h, the alkynyl-functionalized surface-cross-linked micelles (alkynyl-SCM) were formed. Then the reaction mixture was transferred to a glass vial, purged with nitrogen for 15 min, sealed with a rubber stopper, and irradiated in a Rayonet reactor for 12 h. To this mixture compound **3** (10.6 mg, 0.04 mmol), $CuCl_2$ (10 μL of a 6.7 mg/mL solution in H_2O, 0.0005 mmol), and sodium ascorbate (10 μL of a 99 mg/mL solution in H_2O, 0.005 mmol) were added. After being stirred for another 6 h at room temperature, the reaction mixture was poured into acetone (8 mL). The precipitate was collected by centrifugation and washed with a mixture of acetone/water (5 mL/1 mL) three times, methanol/acetic acid (5 mL/0.1 mL) three times, and acetone (6 mL) once before it was dried in air to afford the final MINPs as an off-white powder. Typical yields were ~ 80%.

Preparation of MINPs using functional monomers

A solution of 6-vinylbenzoxaborole (**13**) in methanol was added to template **12** (0.0004 mmol) in a vial containing methanol (5 mL). After the mixture was stirred for 6 h at room temperature, methanol was removed in vacuo. A micellar solution of compound **1** (0.03 mmol), compound **2** (0.02 mmol), divinylbenzene (DVB, 2.8 μL, 0.02 mmol), MBAm (0.02 mmol) and 2,2-dimethoxy-2-phenylacetophenone (DMPA,10 μL of a 12.8 mg/mL solution in DMSO, 0.0005 mmol) in H_2O (2.0 mL) was added to the sugar–boronate complex. The mixture was subjected to ultrasonication for 10 min before $CuCl_2$ (10 μL of a 6.7 mg/mL solution in H_2O, 0.0005 mmol) and sodium ascorbate (10 μL of a 99 mg/mL solution in H_2O, 0.005 mmol) were added. After the reaction mixture was stirred slowly at room temperature for 12 h, the alkynyl-functionalized surface-cross-linked micelles (alkynyl-SCM) were formed. Then the reaction mixture was transferred into a glass vial, purged with

nitrogen for 15 min, sealed with a rubber stopper, and irradiated in a Rayonet reactor for 8 h. Compound **3** (10.6 mg, 0.04 mmol), $CuCl_2$ (10 μL of a 6.7 mg/mL solution in H_2O, 0.0005 mmol), and sodium ascorbate (10 μL of a 99 mg/mL solution in H_2O, 0.005 mmol) were added. After being stirred for another 6 h at room temperature, the reaction mixture was poured into acetone (8 mL). The precipitate collected by centrifugation was washed with a mixture of acetone/water (5 mL/1 mL) three times, methanol/acetic acid (5 mL/0.1 mL) three times, and finally with acetone (1 × 5 mL) once before it was dried in air to afford the final MINPs. Typical yields were ~ 80%.

Determination of Binding Constants by ITC

ITC was performed on a MicroCal VP-ITC Microcalorimeter with Origin 7 software and VPViewer2000 (GE Healthcare, Northampton, MA), following standard procedures.[10,11] In general, a solution of an appropriate guest in Millipore water was injected in equal steps into 1.43 mL of the corresponding MINP in the same solution. The top panel shows the raw calorimetric data. The area under each peak represents the amount of heat generated at each ejection and is plotted against the molar ratio of the MINP to the guest. The smooth solid line is the best fit of the experimental data to the sequential binding of N binding site on the MINP. The heat of dilution for the guest, obtained by titration carried out beyond the saturation point, was subtracted from the heat released during the binding. Binding parameters were auto-generated after curve fitting using Microcal Origin 7.

Dynamic Light Scattering

Particle size of MINP was determined on a Malvern Zetasizer Nano ZS using the Zetasizer software according to the Stokes-Einstein equation (1). The volume of a spherical nanoparticle (V_{D_h}) was calculated from equation (2). Assuming a density of 1.37 g/cm^3 (the density of protein), the molecular weight (MW) of the particle can be calculated using equation (3).[12] A nanoparticle with hydrodynamic diameter of 4.87 nm has a calculated molecular weight of 50 KDa.

$$D_h = \frac{k_B T}{6\pi\eta D_t} \qquad (1)$$

in which D_h is the hydrodynamic diameter, D_t the translational diffusion coefficient measured by dynamic light scattering, T the temperature, k_B the Boltzmann constant, and η is dynamic viscosity of water (0.890 cP at 298 K).

$$V_{D_h} = \frac{4\pi}{3}\left(\frac{D_h}{2}\right)^3 \qquad (2)$$

$$\text{MW in dalton} = \left(\frac{D_h}{0.132}\right)^3 \qquad (3)$$

in which D_h is the hydrodynamic diameter in nm.

[10]Wiseman, T.; Williston, S.; Brandts, J. F.; Lin, L. N. Rapid Measurement of Binding Constants and Heats of Binding Using a New Titration Calorimeter. *Anal. Biochem*. **1989**, 179, 131-137.

[11] Jelesarov, I.; Bosshard, H. R. Isothermal Titration Calorimetry and Differential Scanning Calorimetry as Complementary Tools to Investigate the Energetics of Biomolecular Recognition. *J. Mol. Recognit*. **1999**, 12, 3-18.

[12] Erickson, H. P., Size and shape of protein molecules at the nanometer level determined by sedimentation, gel filtration, and electron microscopy. *Biol. Proced. Online* **2009**, *11*, 32-51.

Table S1. Binding and selectivity data for MINPs prepared with different templates.[a]

entry	guest	K_a ($\times 10^4$ M^{-1})			K_{rel} [b]		
		4a	**4b**	**4c** (n=7)	**4a**	**4b**	**4c** (n=7)
1	maltose	8.41 ± 0.26	7.02 ± 0.45	9.11 ± 0.43	1	1	1
2	maltotriose	0.73 ± 0.05	0.34 ± 0.04	0.21 ± 0.01	0.09	0.05	0.02
3	cellobiose	4.20 ± 0.03	4.31 ± 0.38	4.02 ± 0.25	0.5	0.61	0.44
4	gentiobiose	0.82 ± 0.05	1.15 ± 0.12	0.68 ± 0.06	0.1	0.16	0.07
5	lactose	0.96 ± 0.04	1.21 ± 0.16	0.89 ± 0.04	0.11	0.17	0.10
6	maltulose	0.75 ± 0.03	0.52 ± 0.06	0.46 ± 0.06	0.09	0.07	0.05

[a] The titrations were performed in duplicates with the indicated errors in HEPES buffer (10 mM, pH 7.4) at 298 K. [b] K_{rel} is the binding constant of a guest relative to that of the templating sugar for a particular MINP.

Table S2. Binding and selectivity data for MINP(**11**).[a]

entry	guest	K_a ($\times 10^4$ M^{-1})	-Δ*G* (kcal/mol)	-Δ*H* (kcal/mol)	*T*Δ*S* (kcal/mol)	K_{rel} [b]
1	maltose	0.71 ± 0.10	5.25	0.68 ± 0.05	4.56	0.08
2	maltotriose	0.28 ± 0.03	4.70	0.51 ± 0.09	4.20	0.03
3	cellobiose	5.72 ± 0.32	6.48	0.94 ± 0.07	5.54	0.7
4	gentiobiose	1.79 ± 0.09	5.80	0.78 ± 0.10	5.00	0.22
5	lactose	8.21 ± 0.24	6.70	1.04 ± 0.10	5.66	1
6	maltulose	0.56 ± 0.12	5.11	0.59 ± 0.06	4.53	0.07

[a] The titrations were performed in duplicates with the indicated errors in HEPES buffer (10 mM, pH 7.4) at 298 K. [b] K_{rel} is the binding constant of a guest relative to that of the templating sugar for a particular MINP.

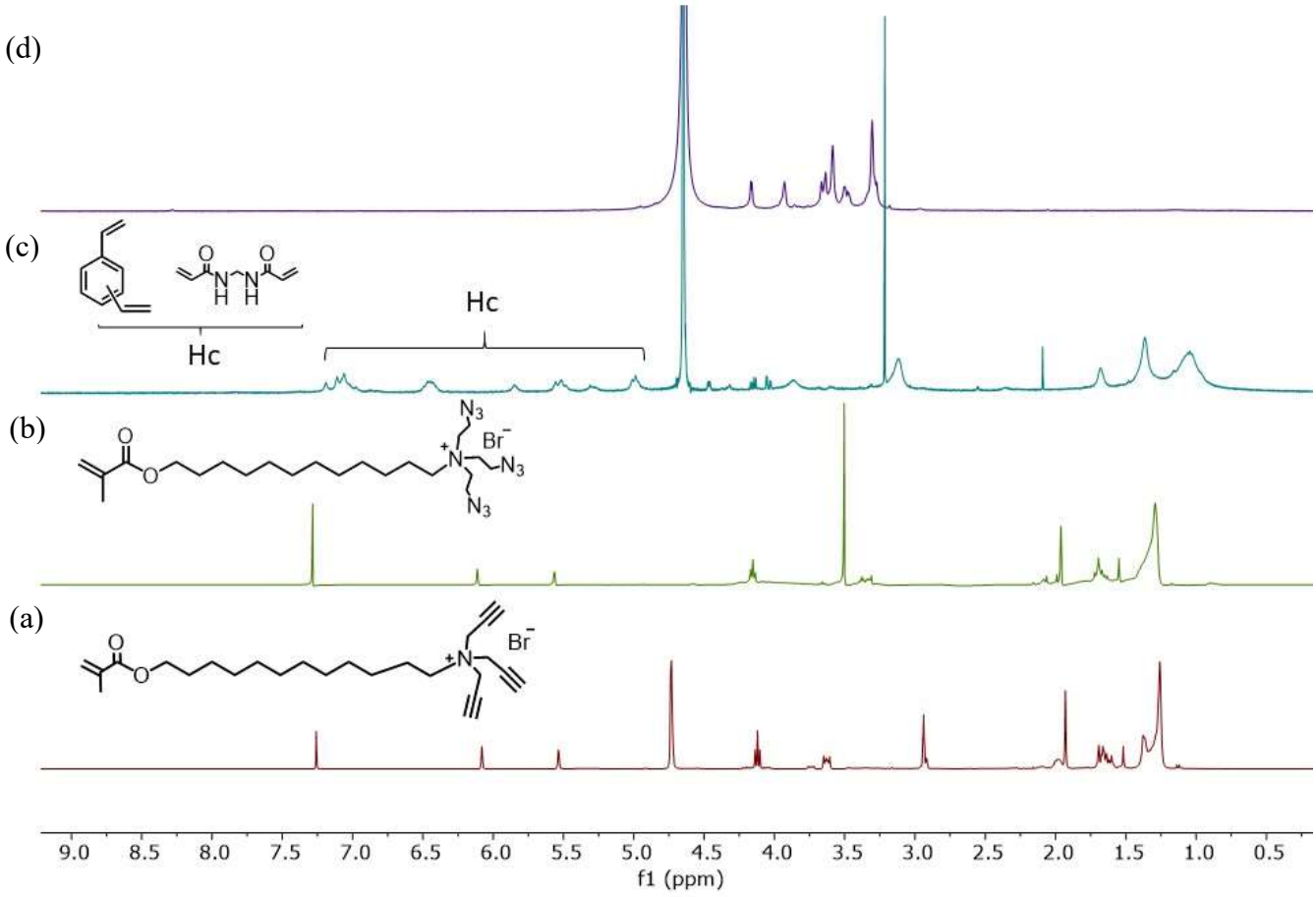

Figure S1. ^{1}H NMR spectra of (a) compound **1** in $CDCl_3$, (b) compound **2** in $CDCl_3$, (c) alkynyl-SCM in D_2O, and (d) MINP(**4a**) in D_2O at 298 K.

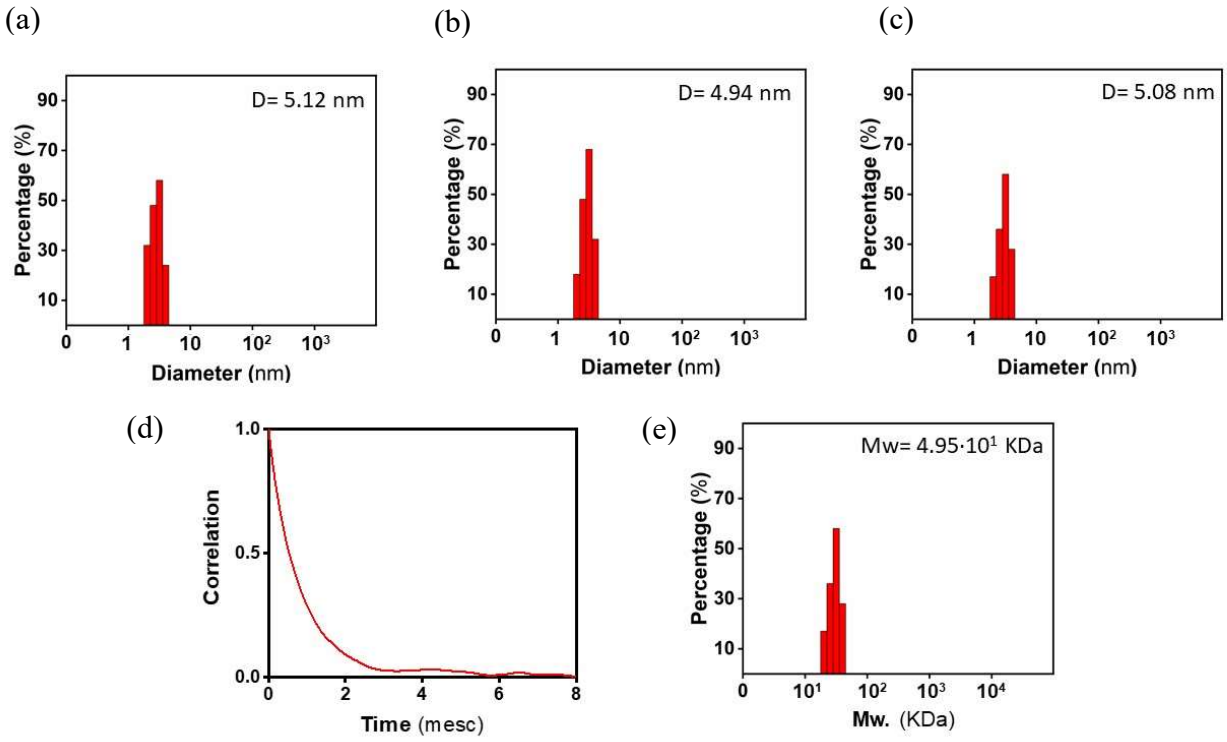

Figure S2. Distribution of the hydrodynamic diameters of the nanoparticles in water at 298 K as determined by DLS for (a) alkynyl-SCM, (b) core cross-linked SCM, and (c) MINP(**4a**) in water. (d) The correlation curve and (e) the corresponding molecular weight of the MINP based on the DLS size. If each unit of building block for the MINP is assumed to contain 0.6 molecule of compound **1** (M_W = 465 g/mol), 0.4 molecules of compound **2** (M_w= 558 g/mol), 0.6 molecules of ligand **3** (MW = 264 g/mol), one molecule of MBAm (MW = 154 g/mol), and one molecule of DVB (Mw= 130g/mol) the molecular weight of the MINP translates to 52 [= 49500 / (0.4×558+ 0.6×465+ 0.6×264+ 130+ 154)] of such units.

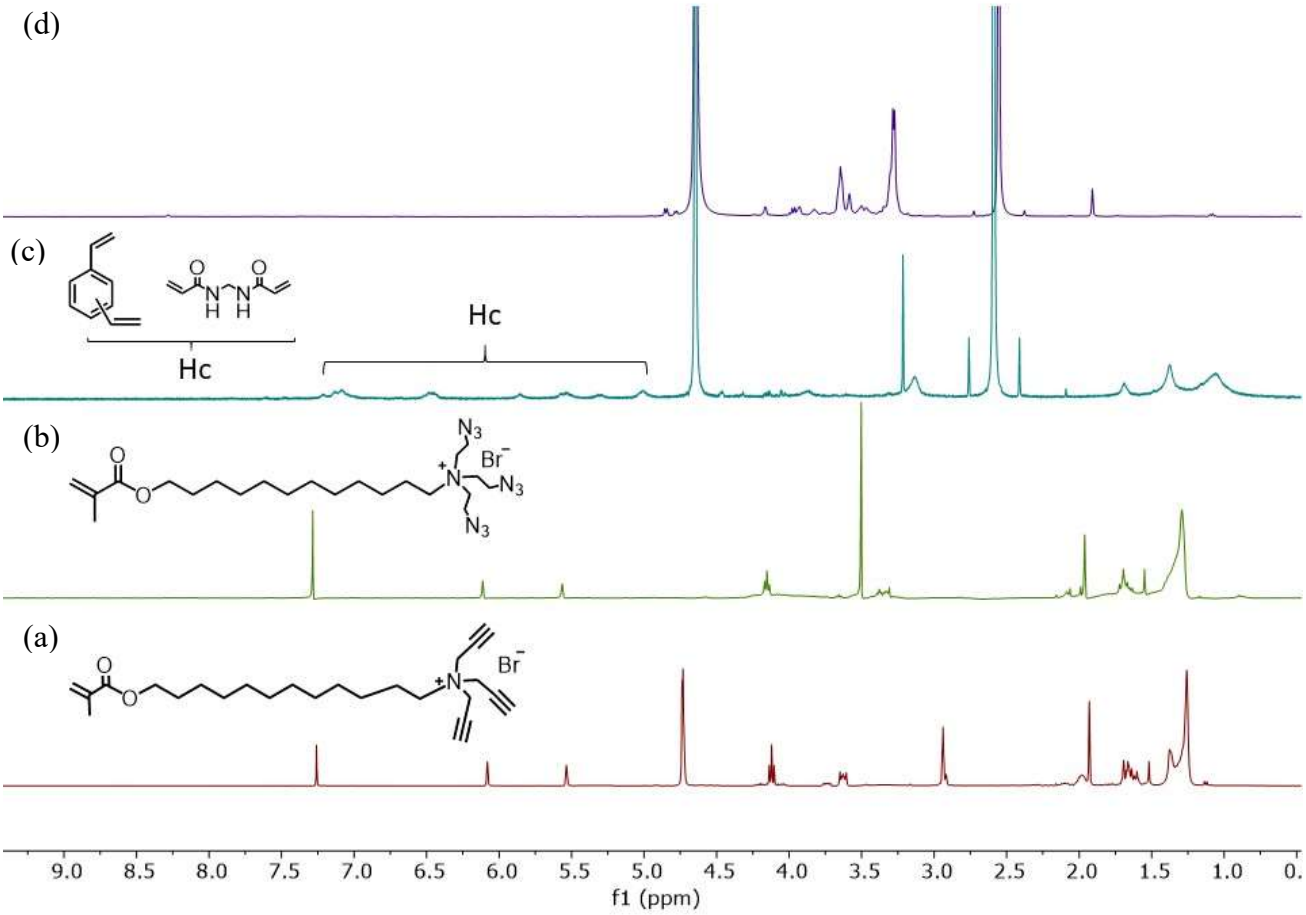

Figure S3. ^{1}H NMR spectra of (a) compound **1** in $CDCl_3$, (b) compound **2** in $CDCl_3$, (c) alkynyl-SCM in D_2O, and (d) MINP(**4b**) in D_2O at 298 K.

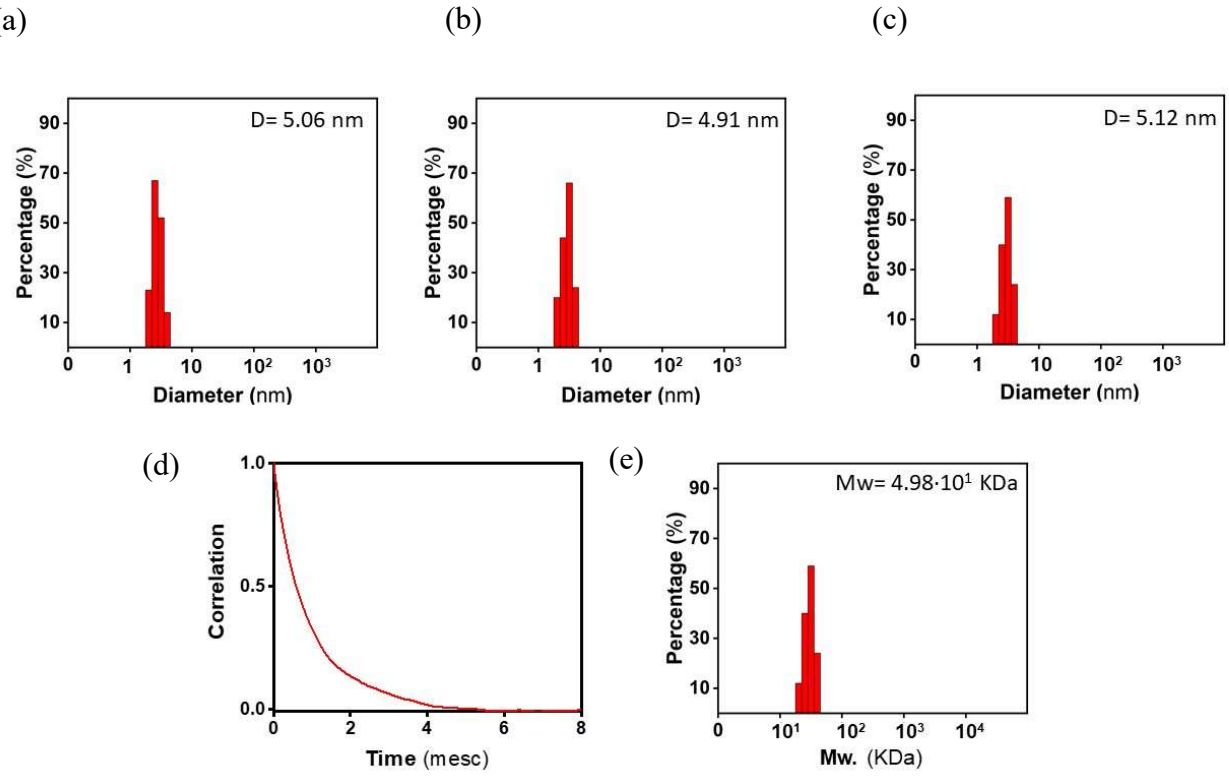

Figure S4. Distribution of the hydrodynamic diameters of the nanoparticles in water at 298 K as determined by DLS for (a) alkynyl-SCM, (b) core cross-linked SCM, and (c) MINP(**4b**) in water. (d) The correlation curve and (e) the corresponding molecular weight of the MINP based on the DLS size. If each unit of building block for the MINP is assumed to contain 0.6 molecule of compound **1** (M_W = 465 g/mol), 0.4 molecules of compound **2** (M_w= 558 g/mol), 0.6 molecules of ligand **3** (MW = 264 g/mol), one molecule of MBAm (MW = 154 g/mol), and one molecule of DVB (Mw= 130g/mol) the molecular weight of the MINP translates to 52 [= 49800 / (0.4×558+ 0.6×465+ 0.6×264+ 130+ 154)] of such units.

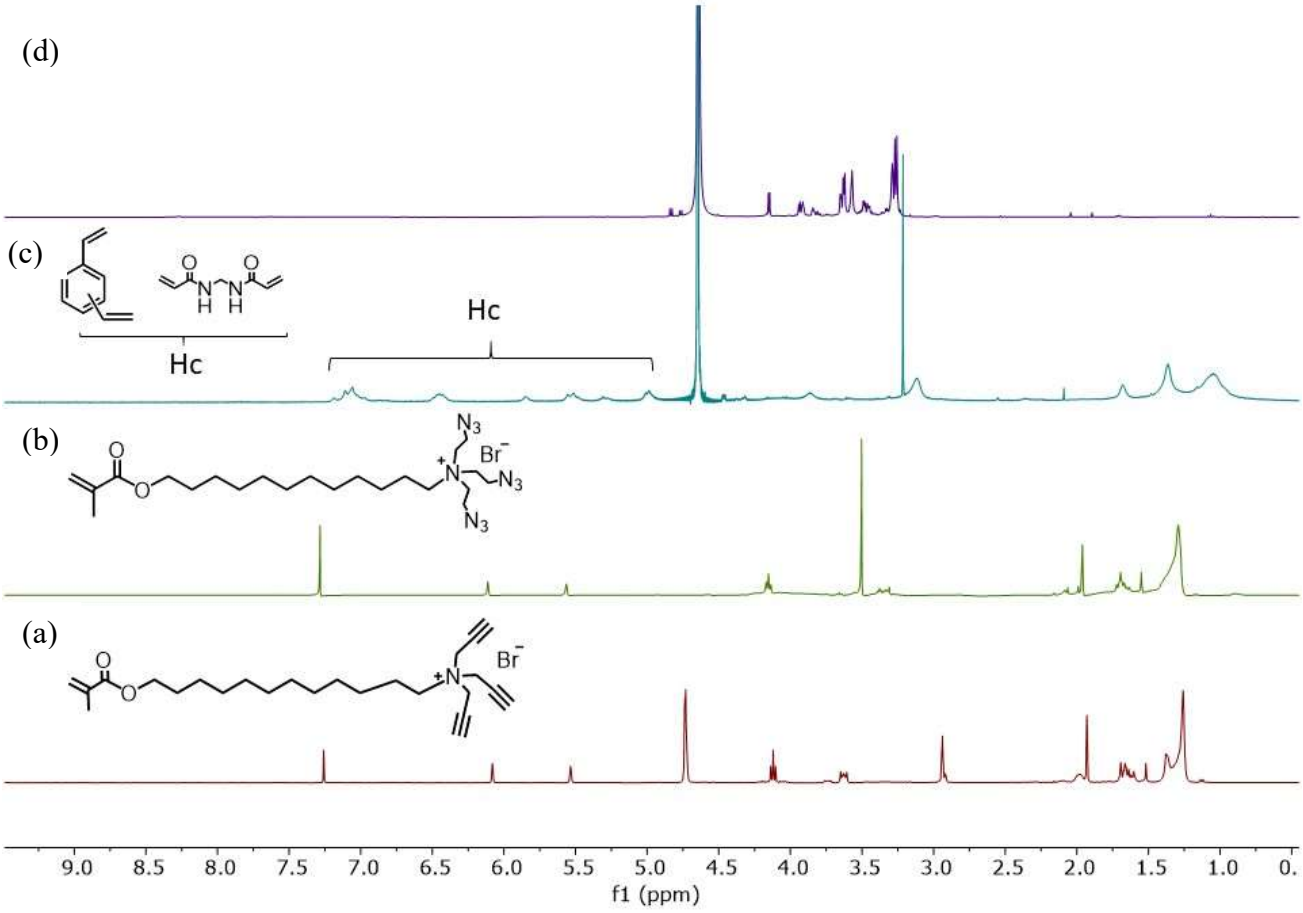

Figure S5. ^{1}H NMR spectra of (a) compound **1** in $CDCl_3$, (b) compound **2** in $CDCl_3$, (c) alkynyl-SCM in D_2O, and (d) MINP(**4c**) in D_2O at 298 K.

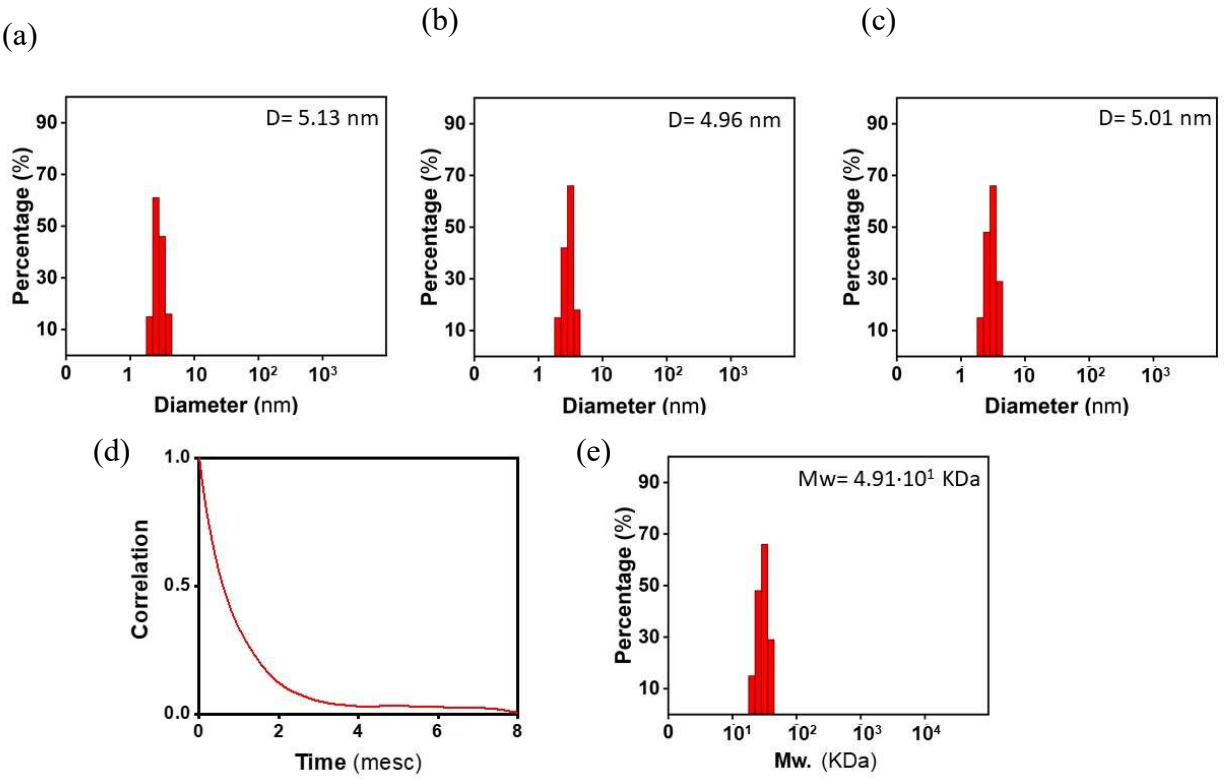

Figure S6. Distribution of the hydrodynamic diameters of the nanoparticles in water at 298 K as determined by DLS for (a) alkynyl-SCM, (b) core cross-linked SCM, and (c) MINP(**4c**) in water. (d) The correlation curve and (e) the corresponding molecular weight of the MINP based on the DLS size. If each unit of building block for the MINP is assumed to contain 0.6 molecule of compound **1** (M_W = 465 g/mol), 0.4 molecules of compound **2** (M_w= 558 g/mol), 0.6 molecules of ligand **3** (MW = 264 g/mol), one molecule of MBAm (MW = 154 g/mol), and one molecule of DVB (Mw= 130g/mol) the molecular weight of the MINP translates to 52 [= 49100 / (0.4×558+ 0.6×465+ 0.6×264+ 130+ 154)] of such units.

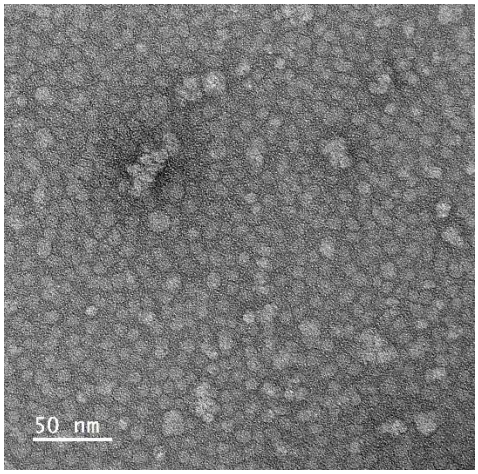

Figure S7. TEM image of typical MINPs. For the TEM imaging, 0.1 mg of MINP was dissolved in 1 mL of Millipore water and the solution was ultra-sonicated for 10 min. A micro syringe was used to load one small drop (~1 μL) of the above solution onto a TEM copper grid covered with carbon film. The sample was left to form a thin layer, and then one small drop (~1 μL) of 2% uranyl acetate solution was loaded on the grid for the negative staining. The sample was left to dry and analyzed on a 200kV JEOL 2100 scanning/transmission electron microscope (STEM).

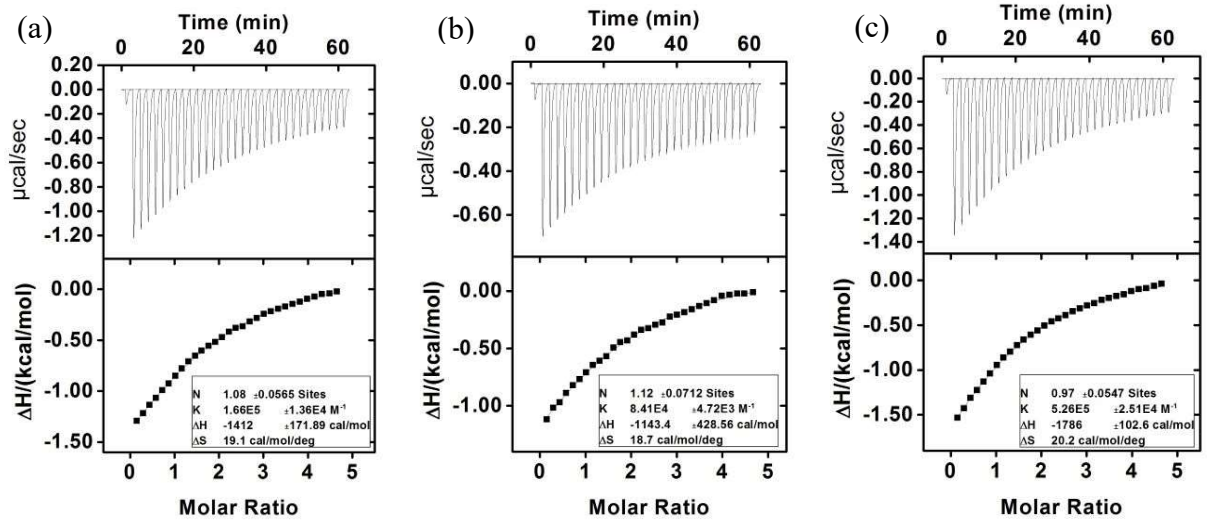

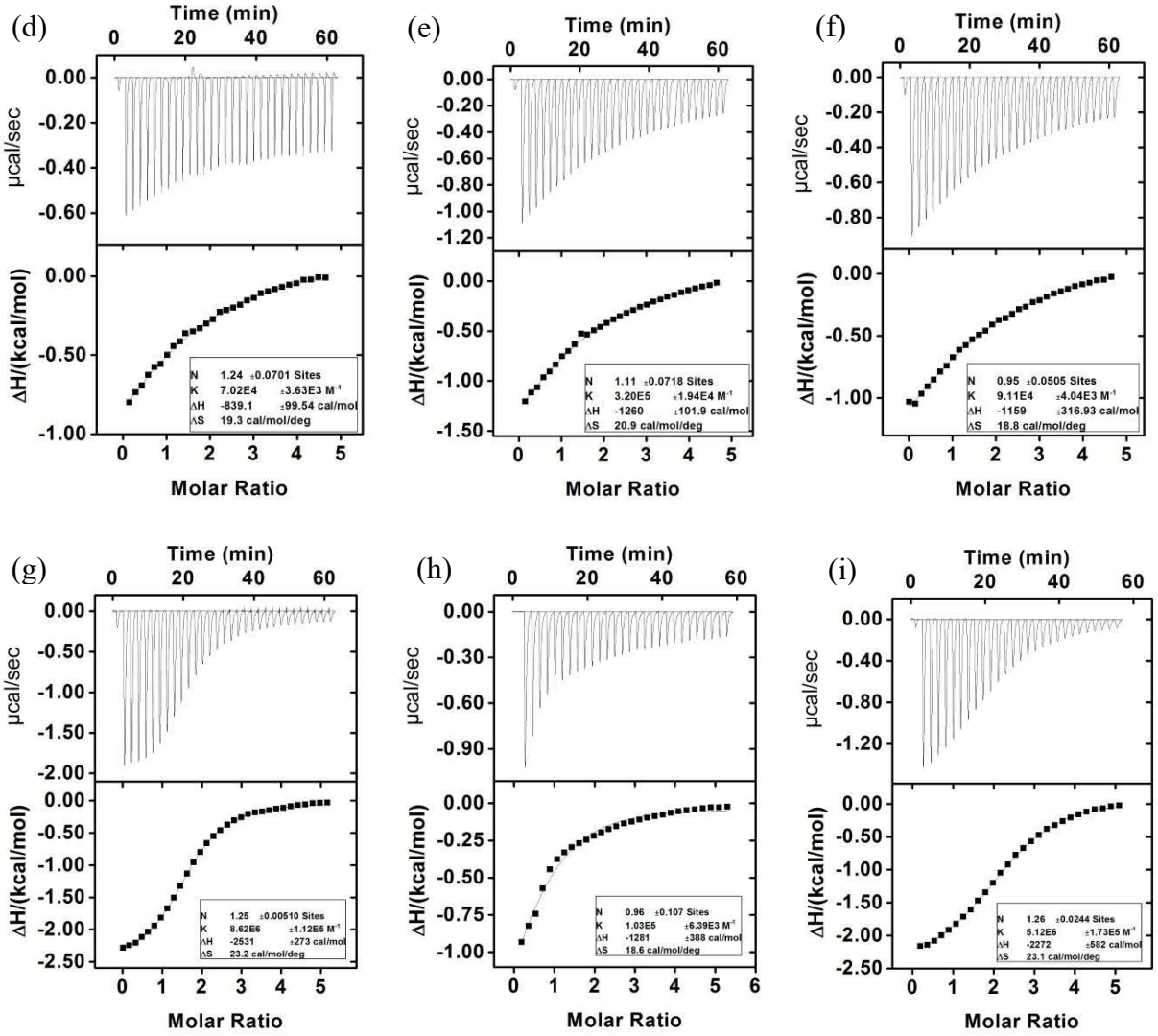

Figure S8. ITC titration curves obtained at 298 K for the titration of MINP(**4a**) with **4a** (a), MINP(**4a**) with maltose (b), MINP(**4b**) with **4b** (c), MINP(**4b**) with maltose (d), MINP(**4c,** n=7) with **4c** n=7 (e), MINP(**4c,** n=7) with maltose (f), MINP(**4d**) with **4d** (g), MINP(**4d**) with maltose (h), and MINP(**4d**) with **15** (i) in 10 mM HEPES buffer (pH 7.4). The data correspond to entries 1-9, respectively, in Table 1. The top panel shows the raw calorimetric data. The area under each peak represents the amount of heat generated at each ejection and is plotted against the molar ratio of MINP to the substrate. The solid line is the best fit of the experimental data to the sequential binding of N equal and independent binding sites on the MINP. The heat of dilution for the substrate, obtained by adding the substrate to the buffer, was subtracted from the heat released during the binding. Binding parameters were auto-generated after curve fitting using Microcal Origin 7.

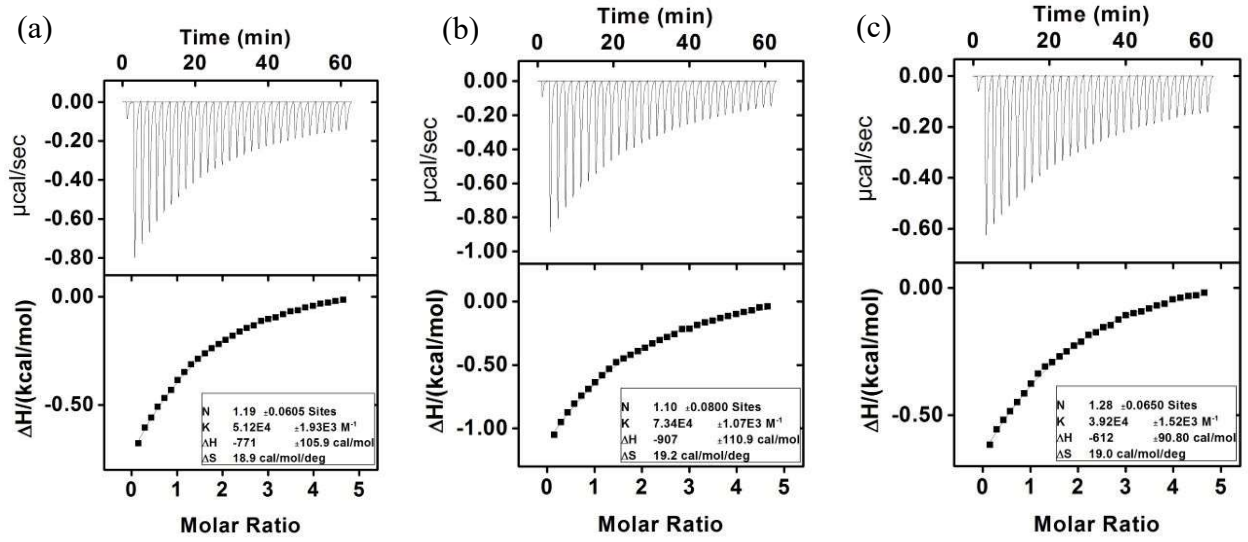

Figure S9. ITC titration curves obtained at 298 K for the titration of MINP(**4c,** n=5) with maltose (a), MINP(**4c,** n=9) with maltose (b), and MINP(**4c,** n=11) with maltose (c) in 10 mM HEPES buffer (pH 7.4). The data correspond to Figure 1a. The top panel shows the raw calorimetric data. The area under each peak represents the amount of heat generated at each ejection and is plotted against the molar ratio of MINP to the substrate. The solid line is the best fit of the experimental data to the sequential binding of N equal and independent binding sites on the MINP. The heat of dilution for the substrate, obtained by adding the substrate to the buffer, was subtracted from the heat released during the binding. Binding parameters were auto-generated after curve fitting using Microcal Origin 7.

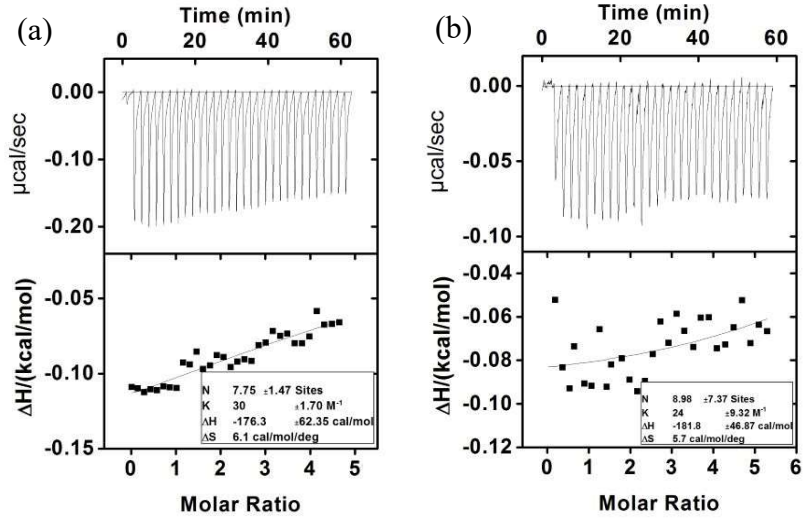

Figure S10. ITC titration curves obtained at 298 K for the titration of MINP(maltose) with maltose (a), and NINP with maltose (b) in 10 mM HEPES buffer (pH 7.4). The data correspond to entries 10 and 11 in Table 1. The top panel shows the raw calorimetric data. The area under each peak represents the amount of heat generated at each ejection and is plotted against the molar ratio of MINP to the substrate. The solid line is the best fit of the experimental data to the sequential binding of N equal and independent binding sites on the MINP. The heat of dilution for the substrate, obtained by adding the substrate to the buffer, was subtracted from the heat released during the binding. Binding parameters were auto-generated after curve fitting using Microcal Origin 7.

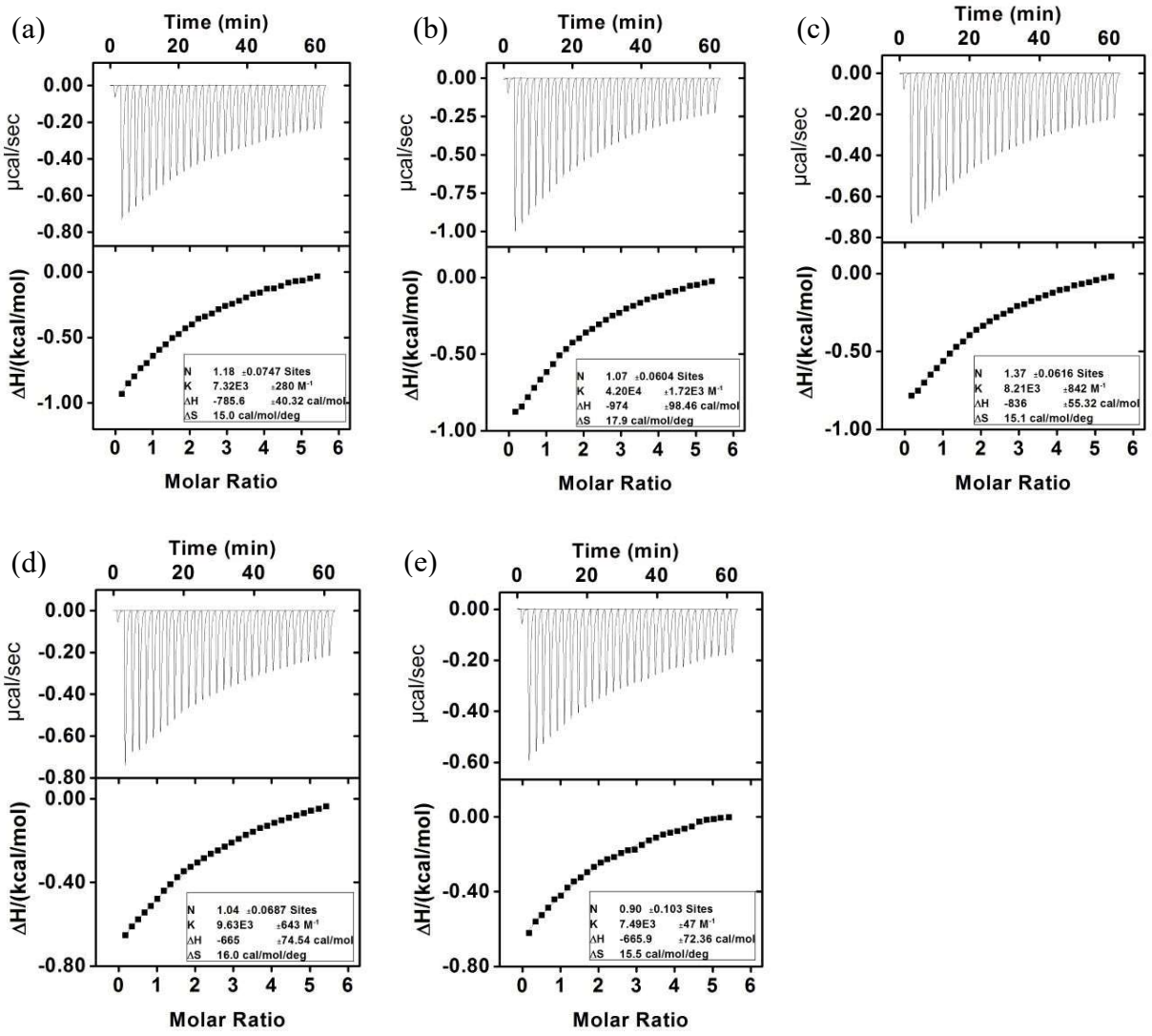

Figure S11. ITC titration curves obtained at 298 K for the titration of MINP(**4a**) with **6** (a), **7** (b), **8** (c), **9** (d), and **10** (e) in 10 mM HEPES buffer (pH 7.4). The data correspond to Figure 1b. The top panel shows the raw calorimetric data. The area under each peak represents the amount of heat generated at each ejection and is plotted against the molar ratio of MINP to the substrate. The solid line is the best fit of the experimental data to the sequential binding of N equal and independent binding sites on the MINP. The heat of dilution for the substrate, obtained by adding the substrate to the buffer, was subtracted from the heat released during the binding. Binding parameters were auto-generated after curve fitting using Microcal Origin 7.

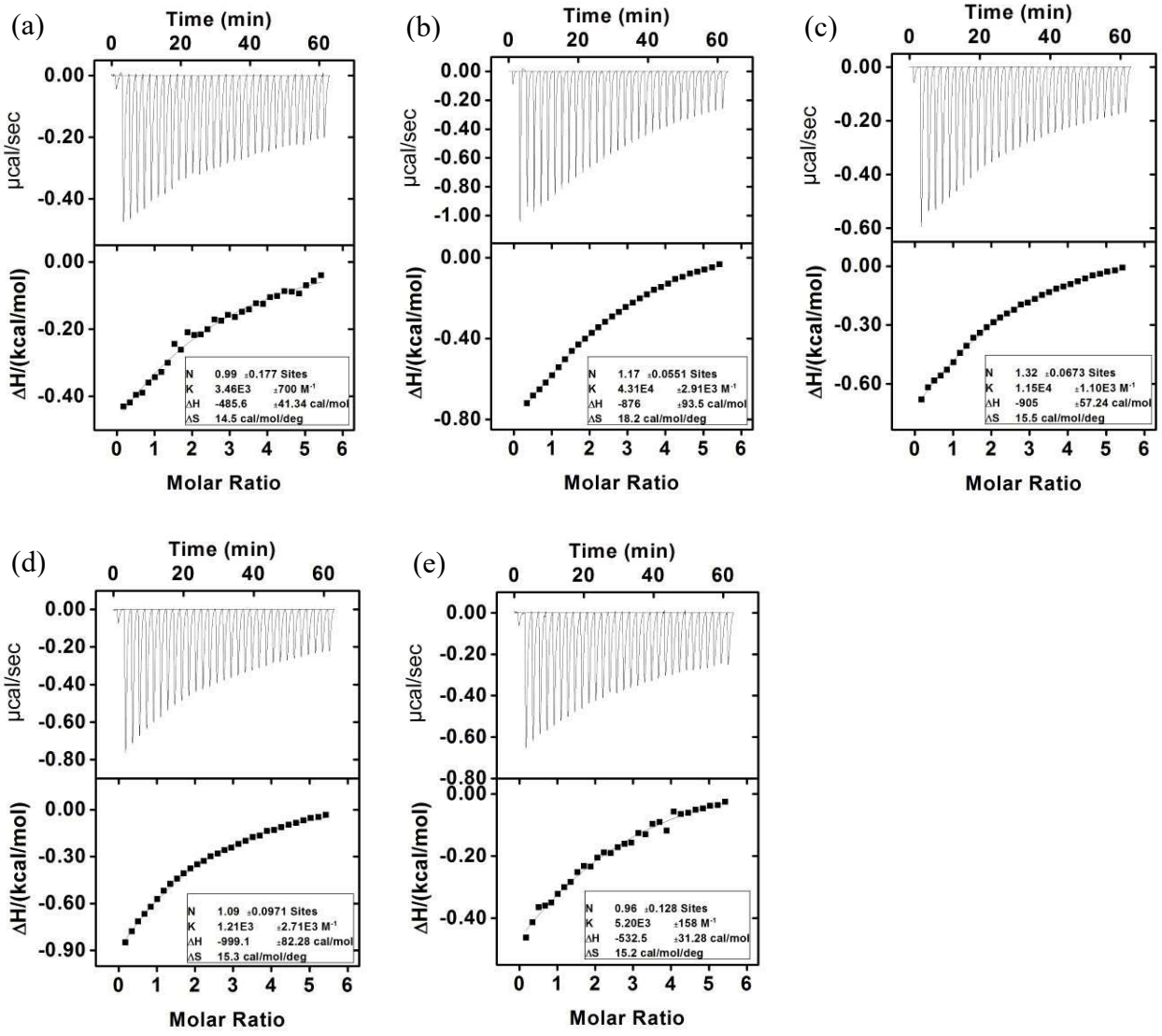

Figure S12. ITC titration curves obtained at 298 K for the titration of MINP(**4b**) with **6** (a), **7** (b), **8** (c), **9** (d), and **10** (e) in 10 mM HEPES buffer (pH 7.4). Data correspond to Figure 1b. The top panel shows the raw calorimetric data. The area under each peak represents the amount of heat generated at each ejection and is plotted against the molar ratio of MINP to the substrate. The solid line is the best fit of the experimental data to the sequential binding of N equal and independent binding sites on the MINP. The heat of dilution for the substrate, obtained by adding the substrate to the buffer, was subtracted from the heat released during the binding. Binding parameters were auto-generated after curve fitting using Microcal Origin 7.

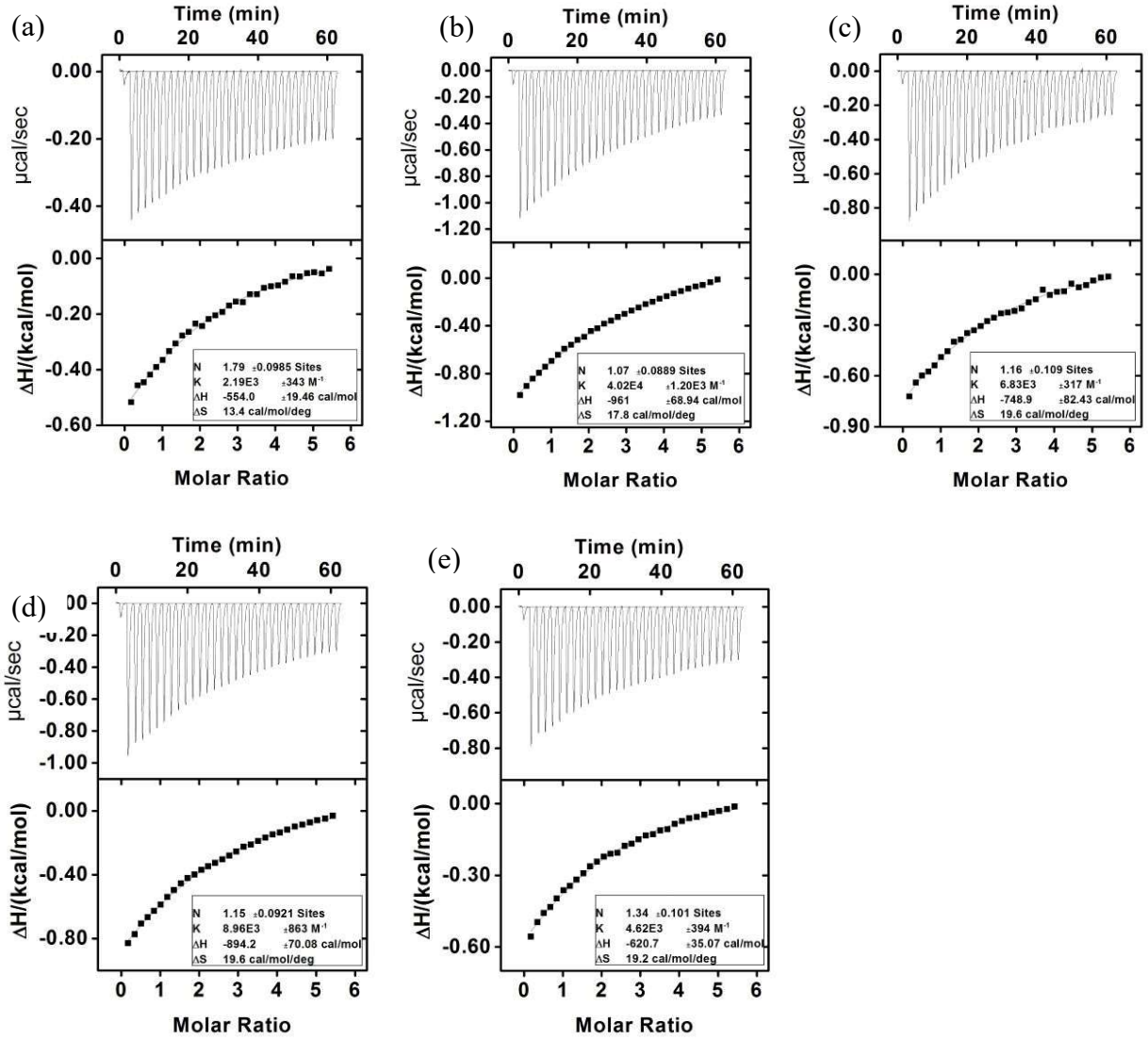

Figure S13. ITC titration curves obtained at 298 K for the titration of MINP(**4c**, n=7) with **6** (a), **7** (b), **8** (c), **9** (d), and **10** (e) in 10 mM HEPES buffer (pH 7.4). The data correspond to blue bars in Figure 1b. The top panel shows the raw calorimetric data. The area under each peak represents the amount of heat generated at each ejection and is plotted against the molar ratio of MINP to the substrate. The solid line is the best fit of the experimental data to the sequential binding of N equal and independent binding sites on the MINP. The heat of dilution for the substrate, obtained by adding the substrate to the buffer, was subtracted from the heat released during the binding. Binding parameters were auto-generated after curve fitting using Microcal Origin 7.

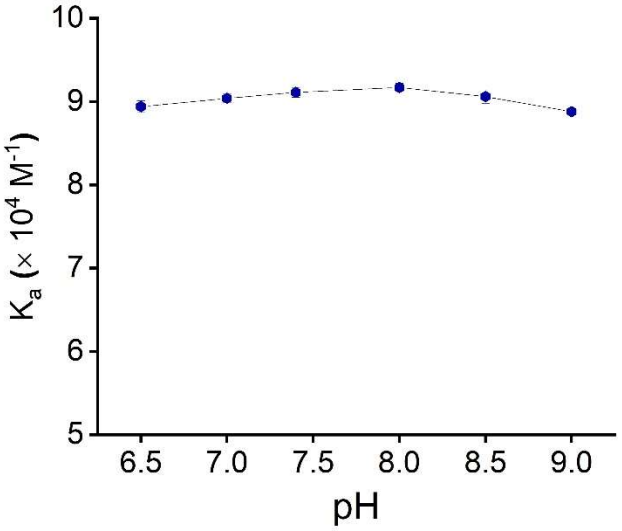

Figure S14. pH effect on the binding of maltose by MINP(**4c**) (n=7).

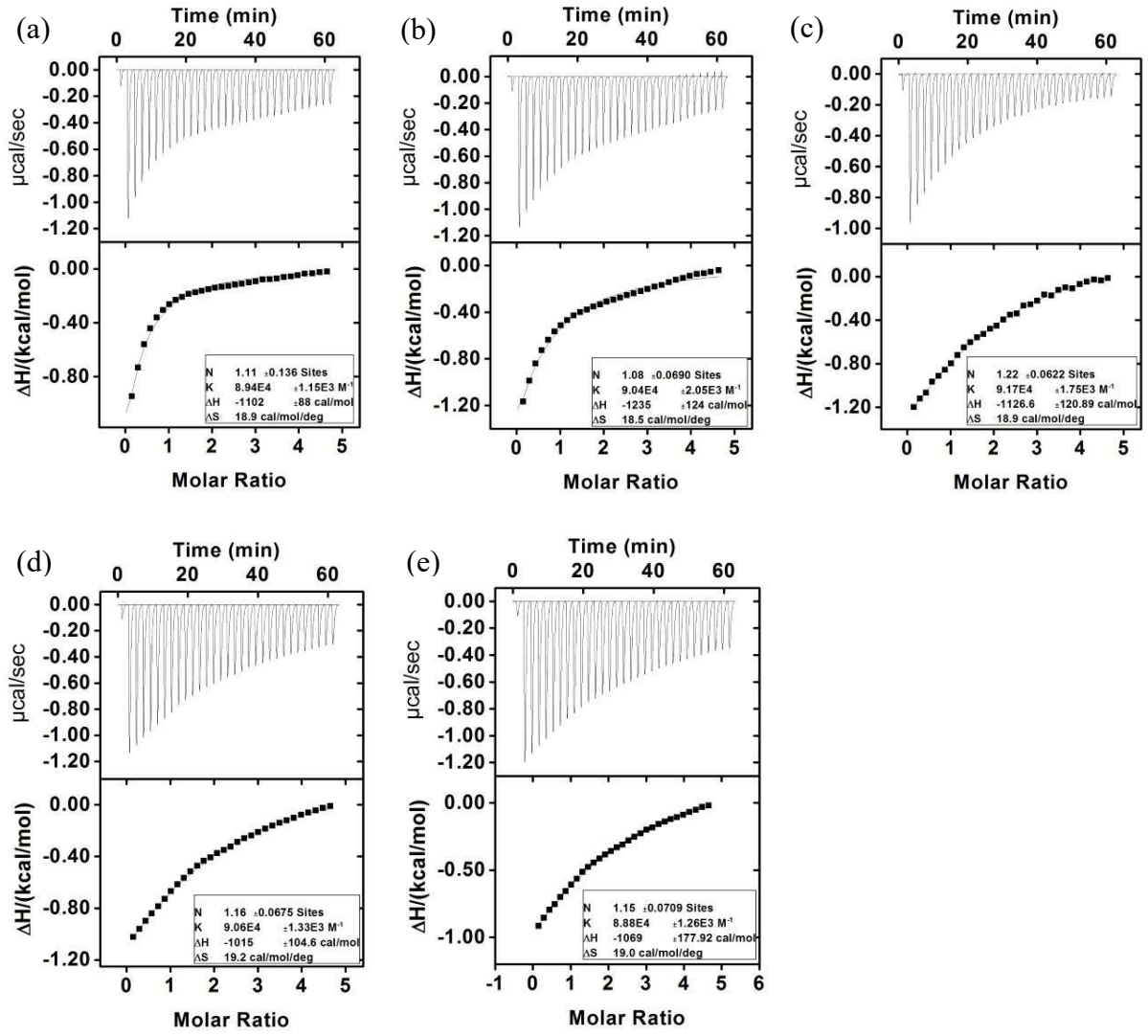

Figure S15. ITC titration curves obtained at 298 K for the titration of MINP(**4c**, n=7) with maltose at pH 6.5 (a), 7 (b), 8 (c), 8.5 (d), and 9 (e). The data correspond to Figure S14. The top panel shows the raw calorimetric data. The area under each peak represents the amount of heat generated at each ejection and is plotted against the molar ratio of MINP to the substrate. The solid line is the best fit of the experimental data to the sequential binding of N equal and independent binding sites on the MINP. The heat of dilution for the substrate, obtained by adding the substrate to the buffer, was subtracted from the heat released during the binding. Binding parameters were auto-generated after curve fitting using Microcal Origin 7.

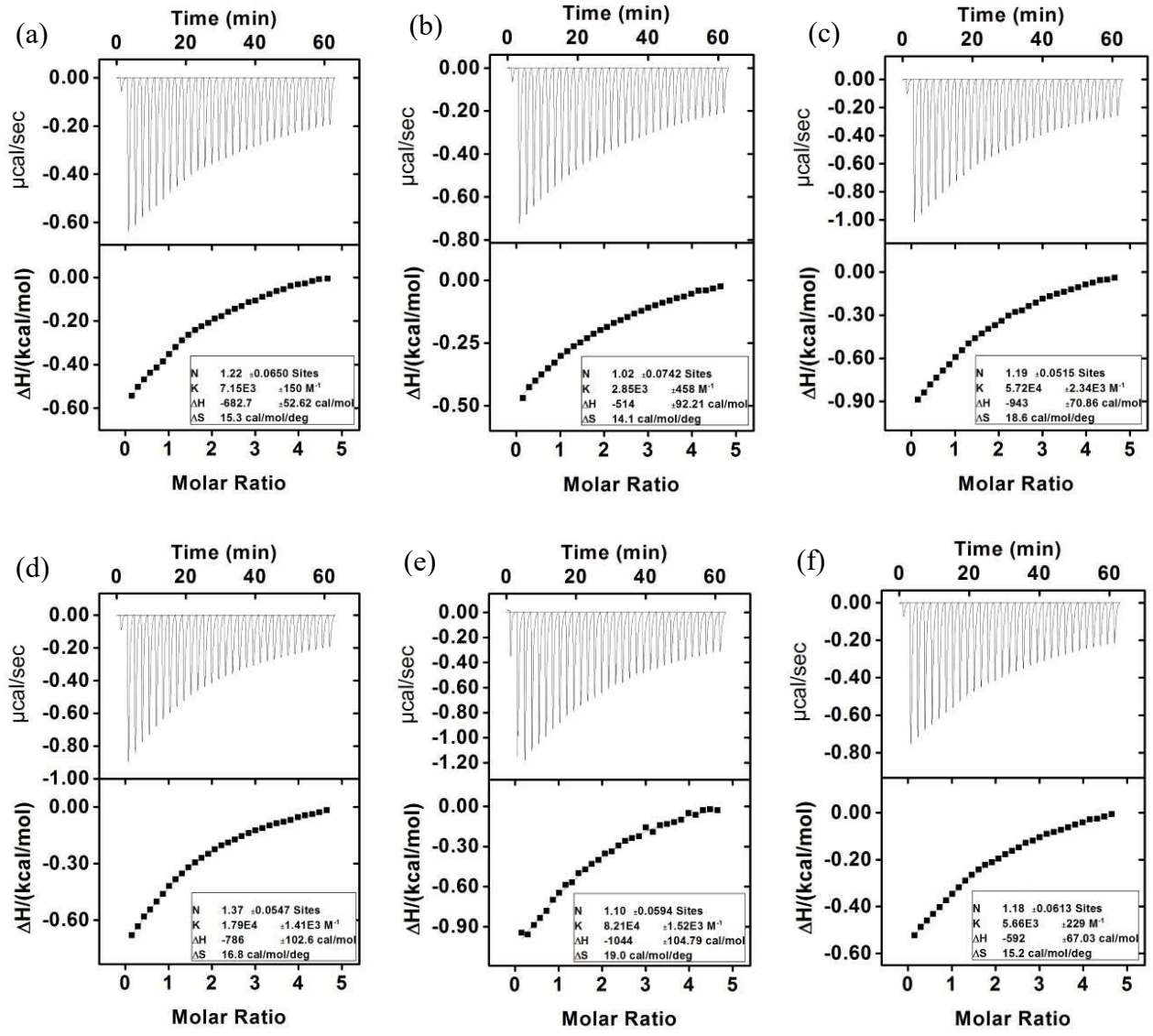

Figure S16. ITC titration curves obtained at 298 K for the titration of MINP(**11**) with **5** (a), **6** (b), **7** (c), **8** (d), **9** (e), and **10** (f) in 10 mM HEPES buffer (pH 7.4). The data correspond Table S2. The top panel shows the raw calorimetric data. The area under each peak represents the amount of heat generated at each ejection and is plotted against the molar ratio of MINP to the substrate. The solid line is the best fit of the experimental data to the sequential binding of N equal and independent binding sites on the MINP. The heat of dilution for the substrate, obtained by adding the substrate to the buffer, was subtracted from the heat released during the binding. Binding parameters were auto-generated after curve fitting using Microcal Origin 7.

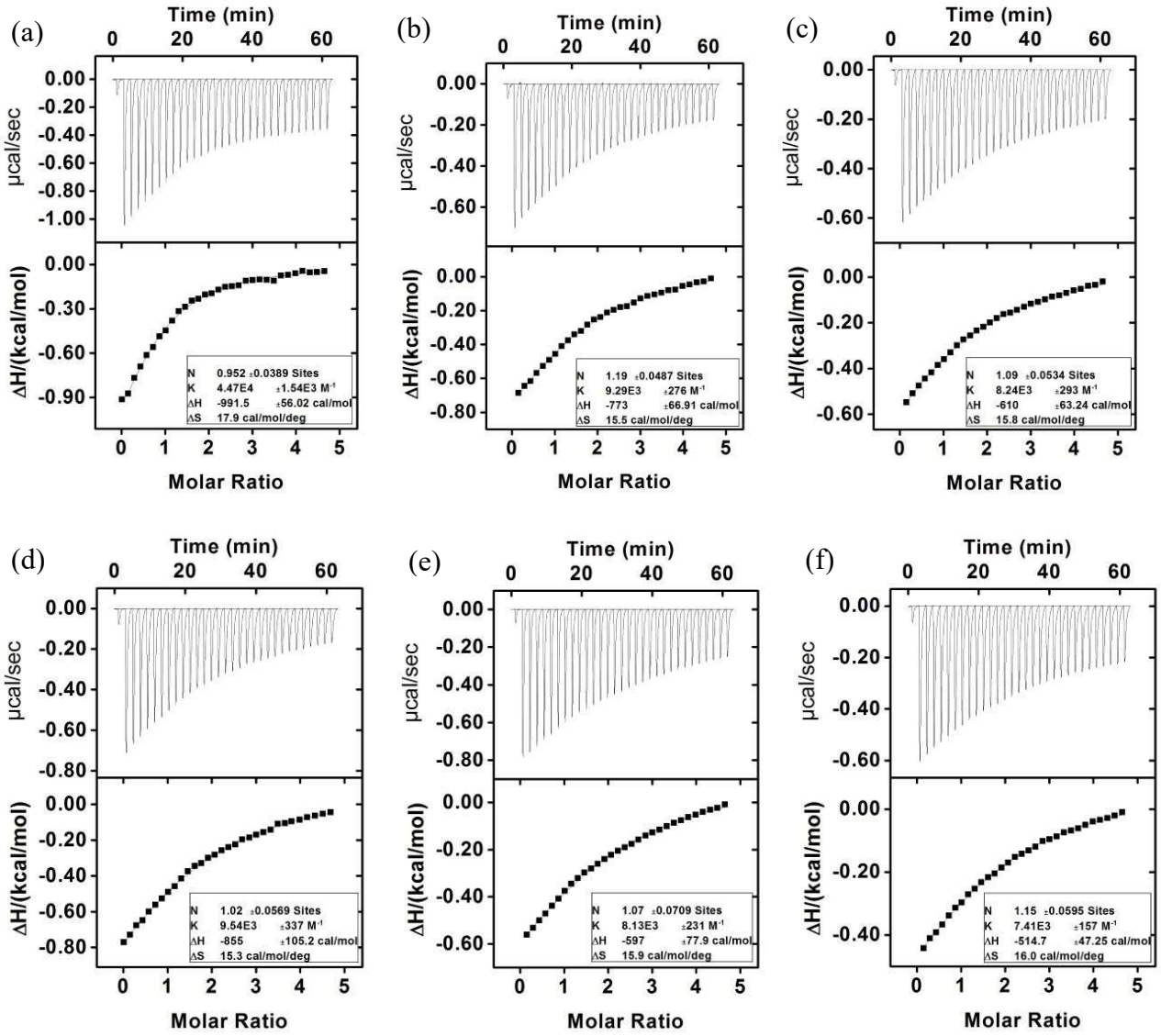

Figure S17. ITC titration curves obtained at 298 K for the titration of MINP(**12**) with **6** (a), **5** (b), **7** (c), **8** (d), **9** (e), and **10** (f) in 10 mM HEPES buffer (pH 7.4). The data correspond Table 2. The top panel shows the raw calorimetric data. The area under each peak represents the amount of heat generated at each ejection and is plotted against the molar ratio of MINP to the substrate. The solid line is the best fit of the experimental data to the sequential binding of N equal and independent binding sites on the MINP. The heat of dilution for the substrate, obtained by adding the substrate to the buffer, was subtracted from the heat released during the binding. Binding parameters were auto-generated after curve fitting using Microcal Origin 7.

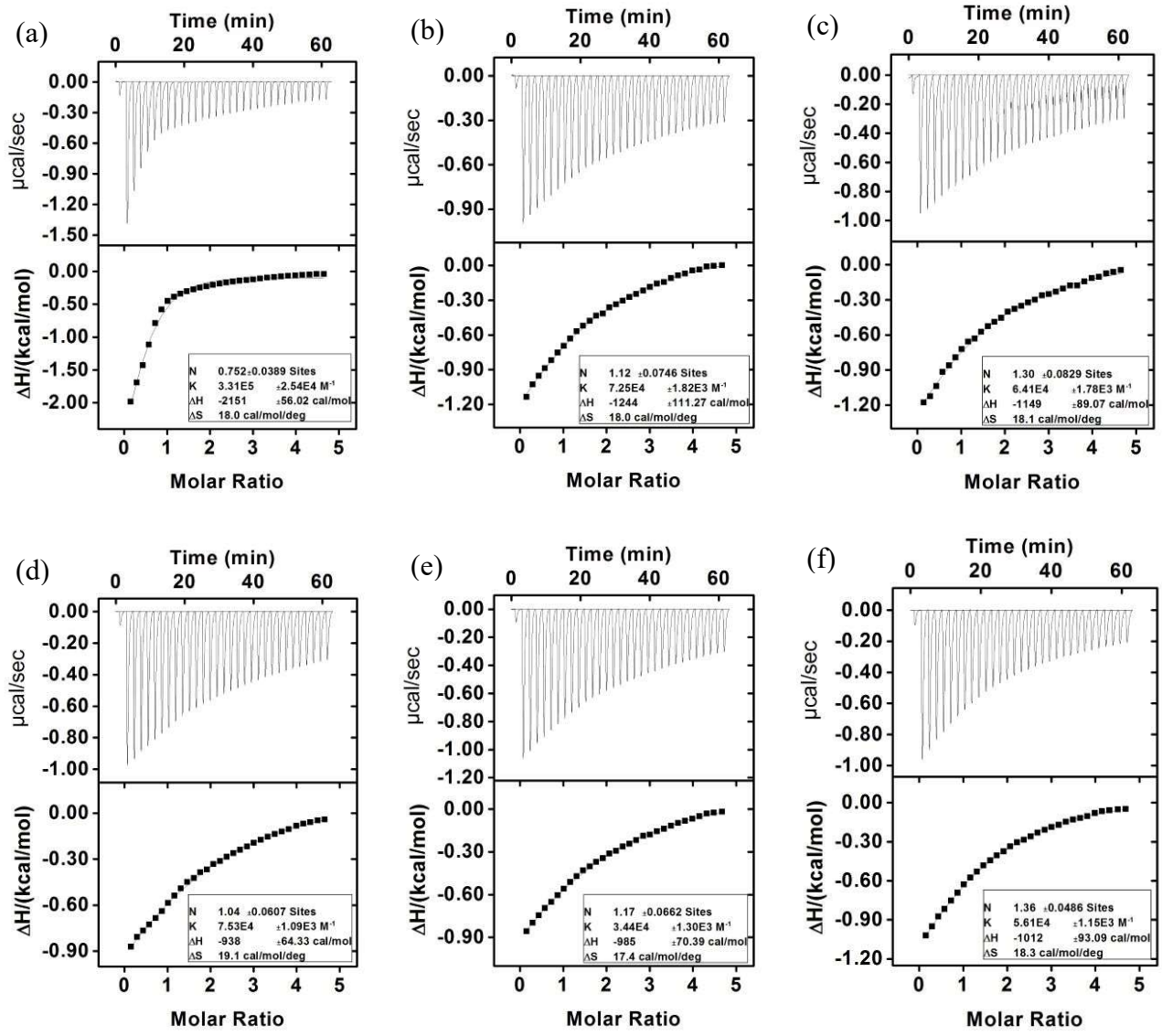

Figure S18. ITC titration curves obtained at 298 K for the titration of MINP(**14**) with **6** (a), **5** (b), **7** (c), **8** (d), **9** (e), and **10** (f) in 10 mM HEPES buffer (pH 7.4). The data correspond to Table 2. The top panel shows the raw calorimetric data. The area under each peak represents the amount of heat generated at each ejection and is plotted against the molar ratio of MINP to the substrate. The solid line is the best fit of the experimental data to the sequential binding of N equal and independent binding sites on the MINP. The heat of dilution for the substrate, obtained by adding the substrate to the buffer, was subtracted from the heat released during the binding. Binding parameters were auto-generated after curve fitting using Microcal Origin 7.

Maltose hydrolysis experiment

A solution of maltose (10 μM) and maltase (10 units) in 1 mL phosphate buffer (100 mM, pH 6.8) was incubated at 37 ºC for the designated time in the presence or absence of different MINPs. After the reaction mixture was centrifuged to remove the MINPs, the amount of produced glucose in the supernatant solution was measured using an enzymatic commercial glucose assay kit. Similar procedures were followed in Figure 3 with different concentrations of maltose and MINP(**4d**) used and 25 μM of deprotecting ligand **15** added at 5, 15, 25, and 35 min.

Glucose produced from the hydrolysis of oligosaccharides was measured enzymatically by a commercial glucose assay kit. Aliquots of the above hydrolysis solution (250 μL), Tris buffer (750 μL, 50 mM Tris, pH = 7.5), the enzyme solution (500 μL, 10 units/mL of hexokinase/glucose-6-phosphoate dehydrogenase and 1 mM ATP dissolved in the above Tris buffer), and NAD solution (500 μL, 1 mM dissolved in the above Tris buffer) were incubated at room temperature for 15 minutes. The absorbance of NADH at 340 nm was monitored. This absorbance was used to calculate the amount of glucose in the solution based on the following equation

$$[\text{glucose}] = (A_t - A_b) \times V_t \times F \times 0.029/V_s$$

in which A_t and A_b are the tested and blank absorbance respectively, V_t the total volume, F the dilution factor, and V_s the sample volume.

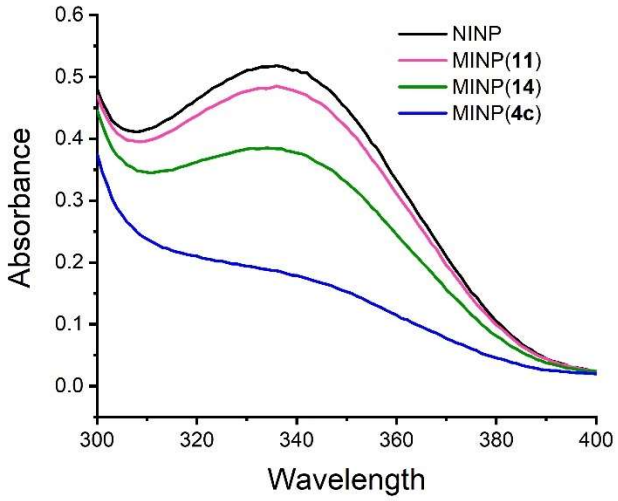

Figure S19. A sample UV absorbance graph generated by using the glucose assay kit for maltose hydrolysis experiment in the presence of different MINPs. [maltose] = 10 μM. [NINP] = [MINP] = 10 μM. [maltase] = 10 units/mL incubated in 1 mL of phosphate buffer (100 mM, pH 6.8) at 37 ºC for 20 min.

Maltotetraose hydrolysis experiment

A solution of maltotetraose (20 μM) and maltase (10 units) in 1 mL phosphate buffer (100 mM, pH 6.8) was incubated at 37 ºC in the presence of different nanoparticles (40 μM). After 2 h, the reaction mixture was centrifuged at 20,000 RPM for 10 min to remove the nanoparticles. Analysis of reaction mixture after hydrolysis was performed by LC-MS analysis using an Agilent 1200 Series Binary VWD system with an Agilent 6540 UHD Accurate Mass Q-TOF mass detector. Separation of the products was performed on a Thermo Scientific HILIC-LC column (4.6 mm, 150 mm) at 60 ºC. The

concentrations of produced glucose, maltose and maltotriose in the supernatant solution were measured using calibration curves generated from authentic samples.

NMR and mass spectra

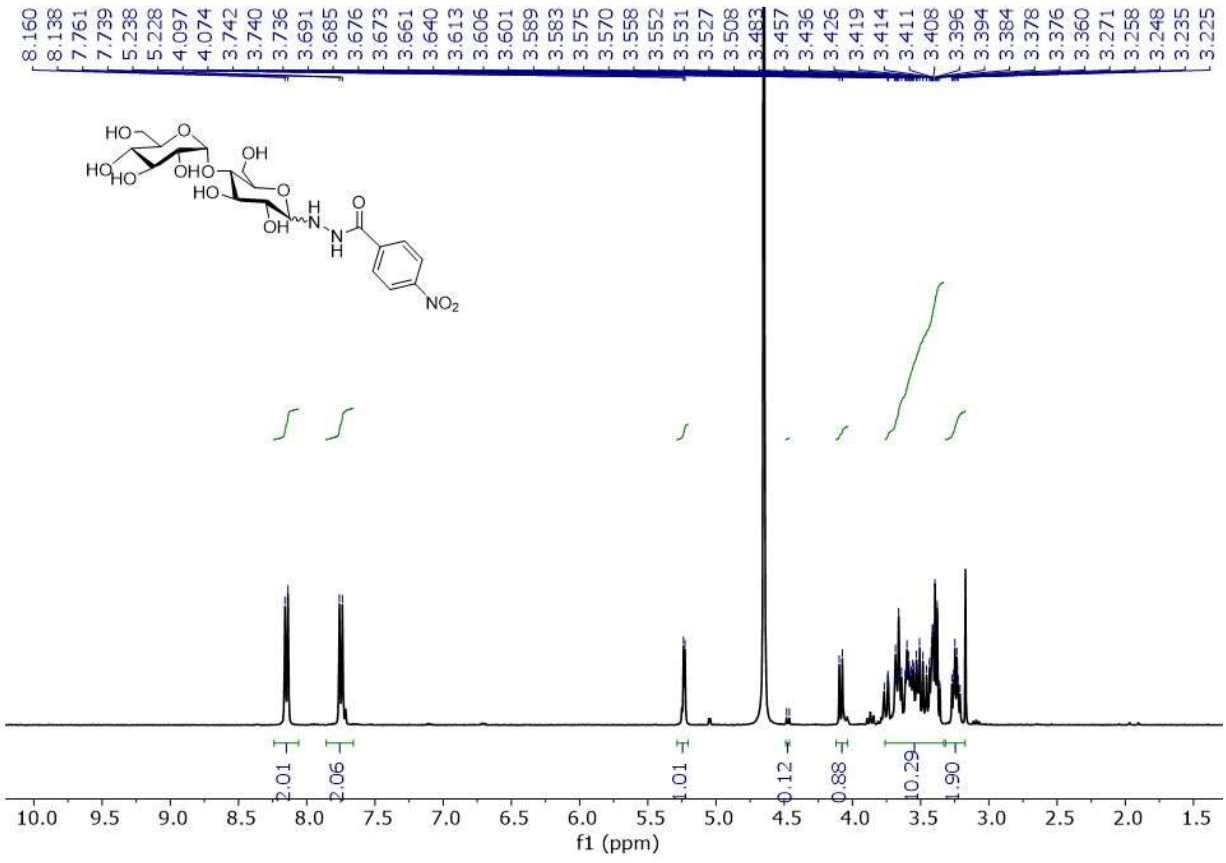

Figure S20. ^{1}H NMR spectrum of **4a** in D_2O.

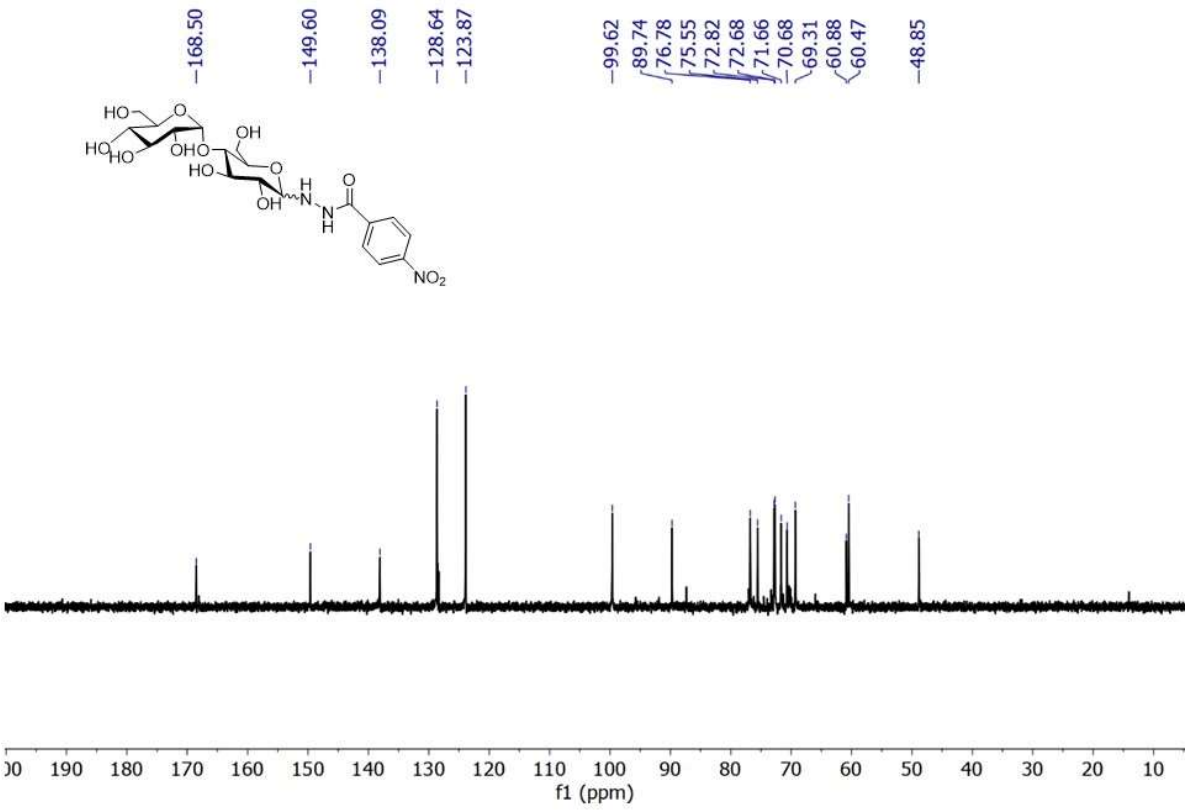

Figure S21. ^{13}C NMR spectrum of **4a** in D_2O.

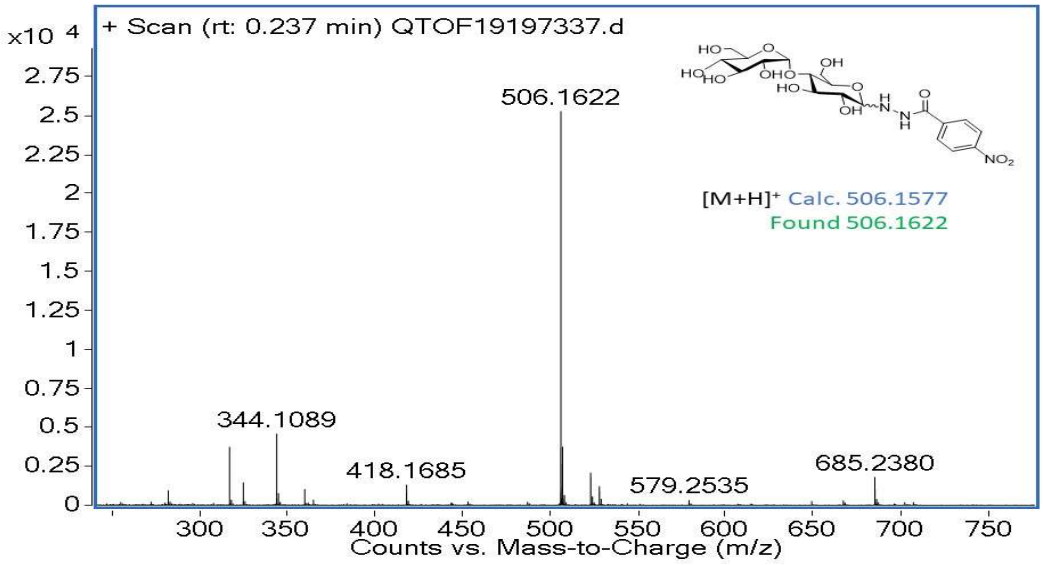

Figure S22. Mass spectrum of **4a**.

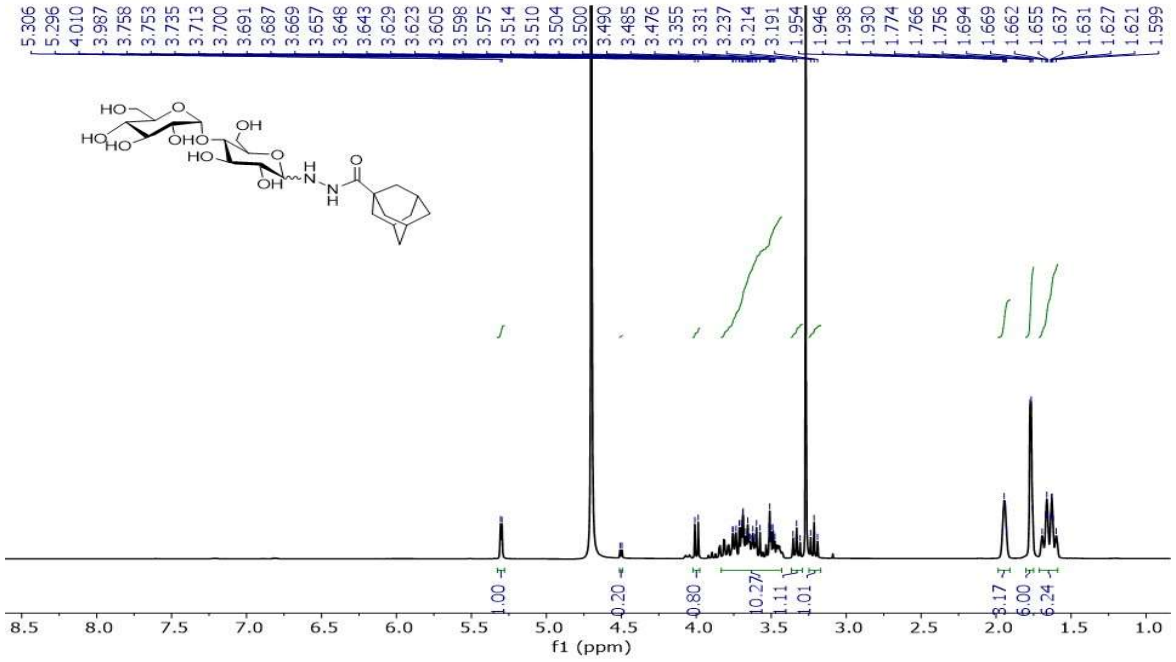

Figure S23. ^{1}H NMR spectrum of **4b** in D_2O.

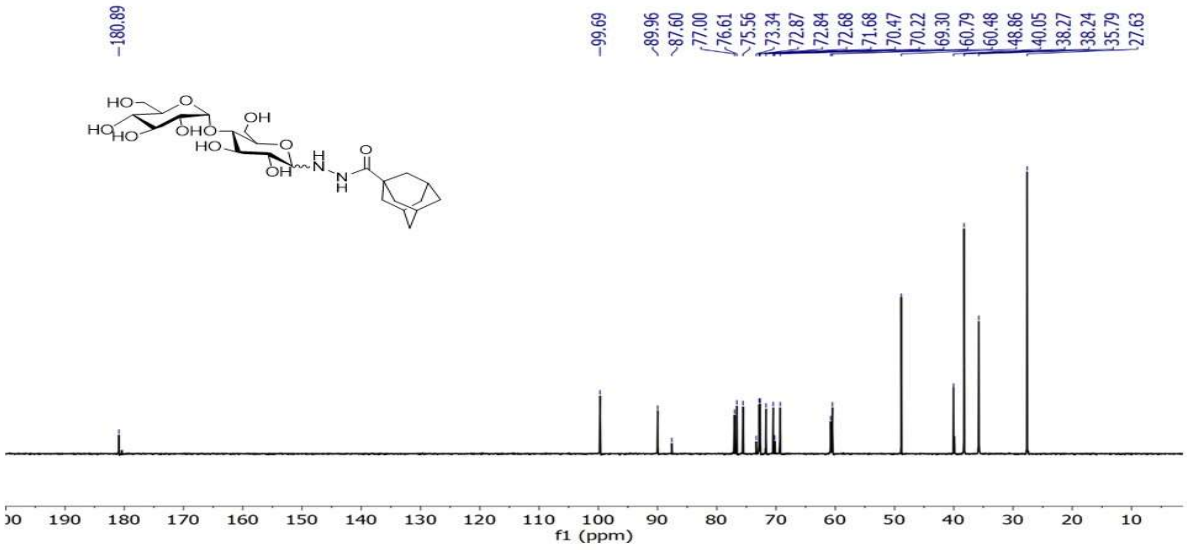

Figure S24. ^{13}C NMR spectrum of **4b** in D_2O.

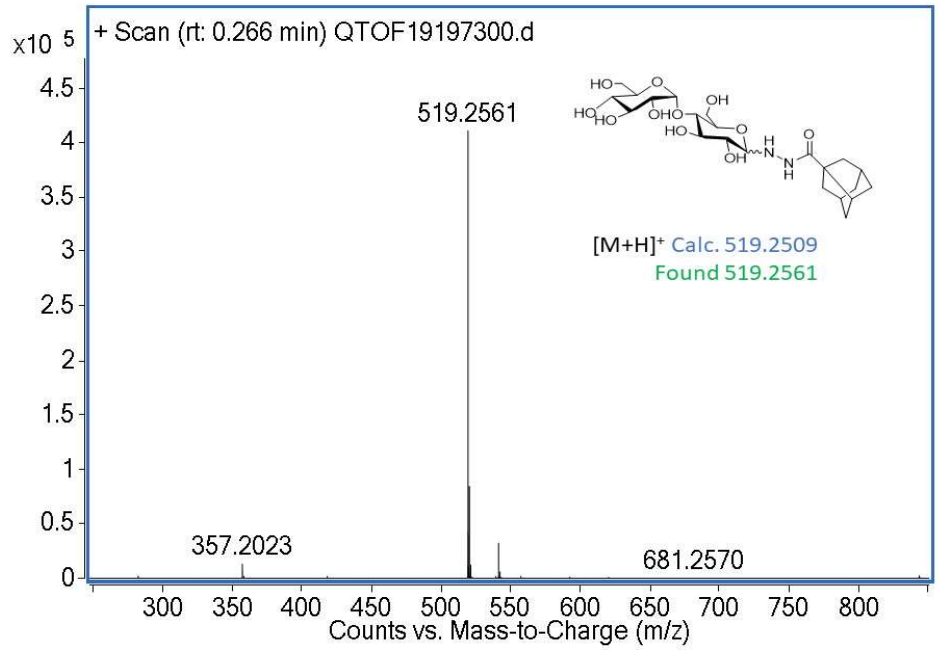

Figure S25. Mass spectrum of **4b**.

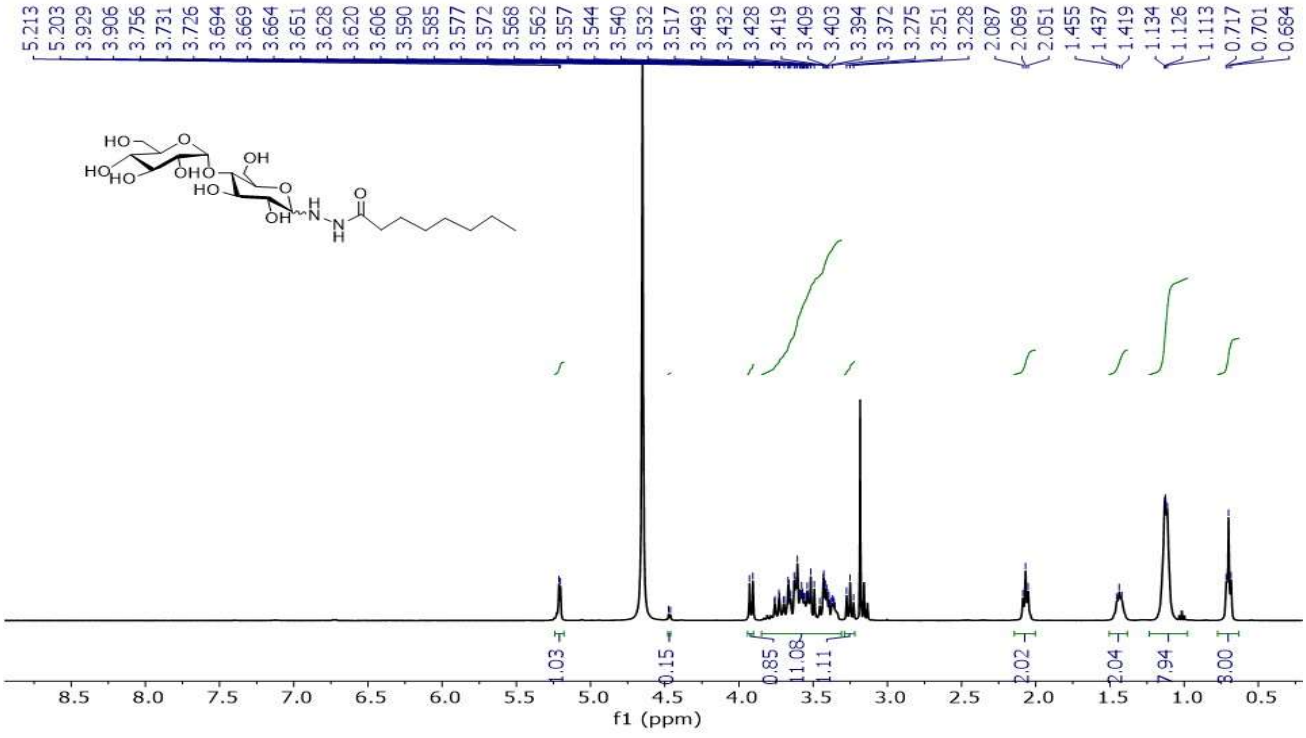

Figure S26. ^{1}H NMR spectrum of **4c** (n = 7) in D_2O. (The labeled peaks are related to the residual diethyl ether used in the last step of purification.)

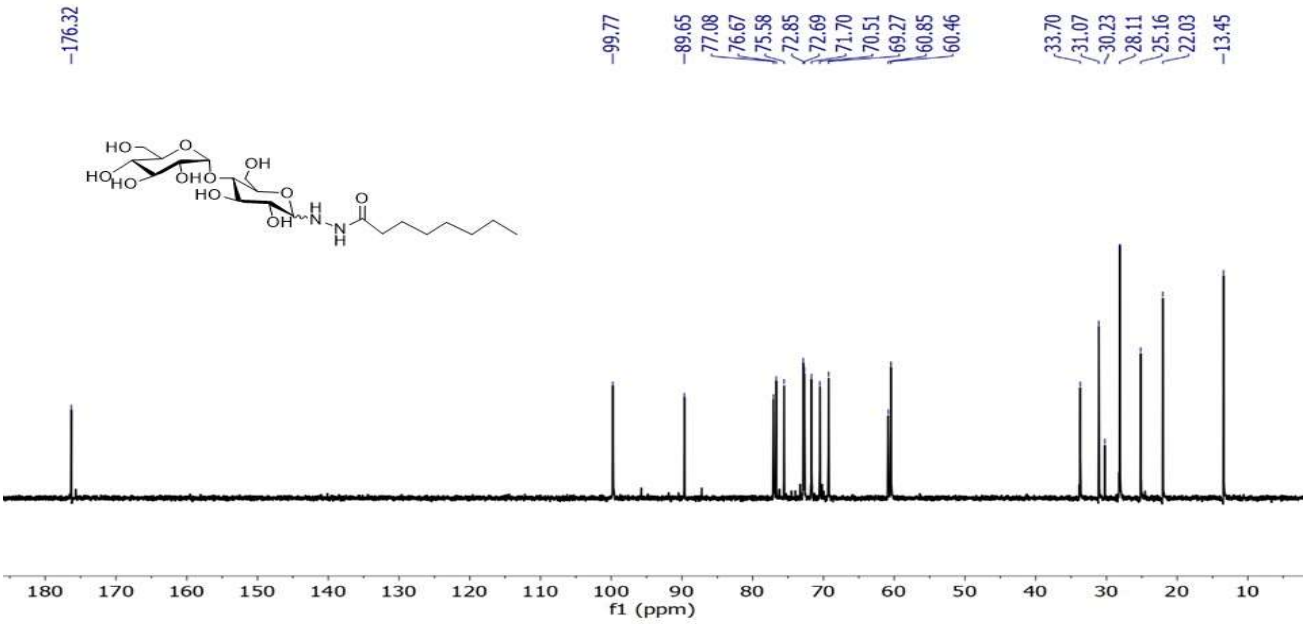

Figure S27. ^{13}C NMR spectrum of **4c** (n = 7) in D_2O.

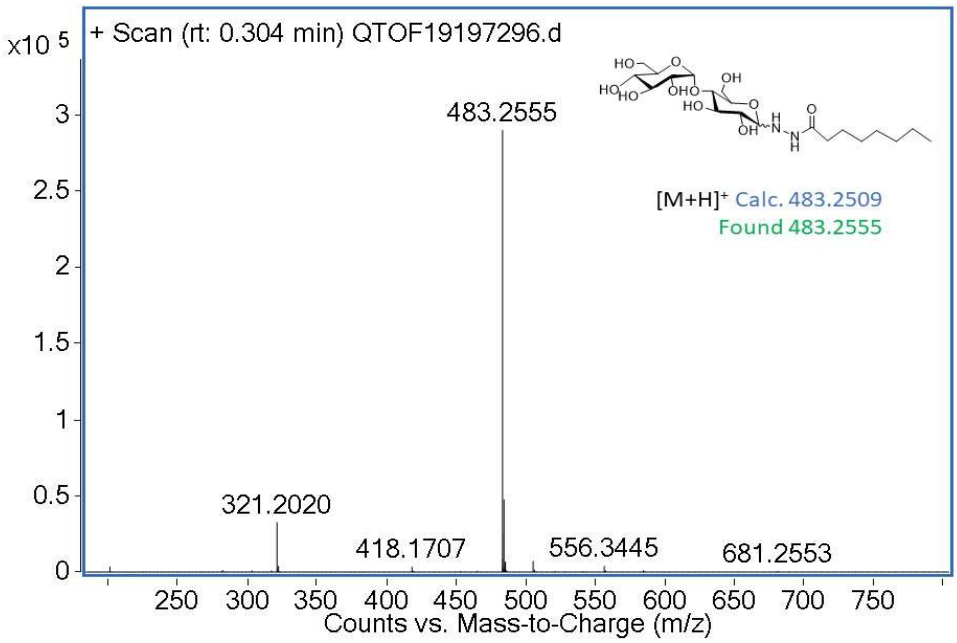

Figure S28. Mass spectrum of **4c** (n = 7).

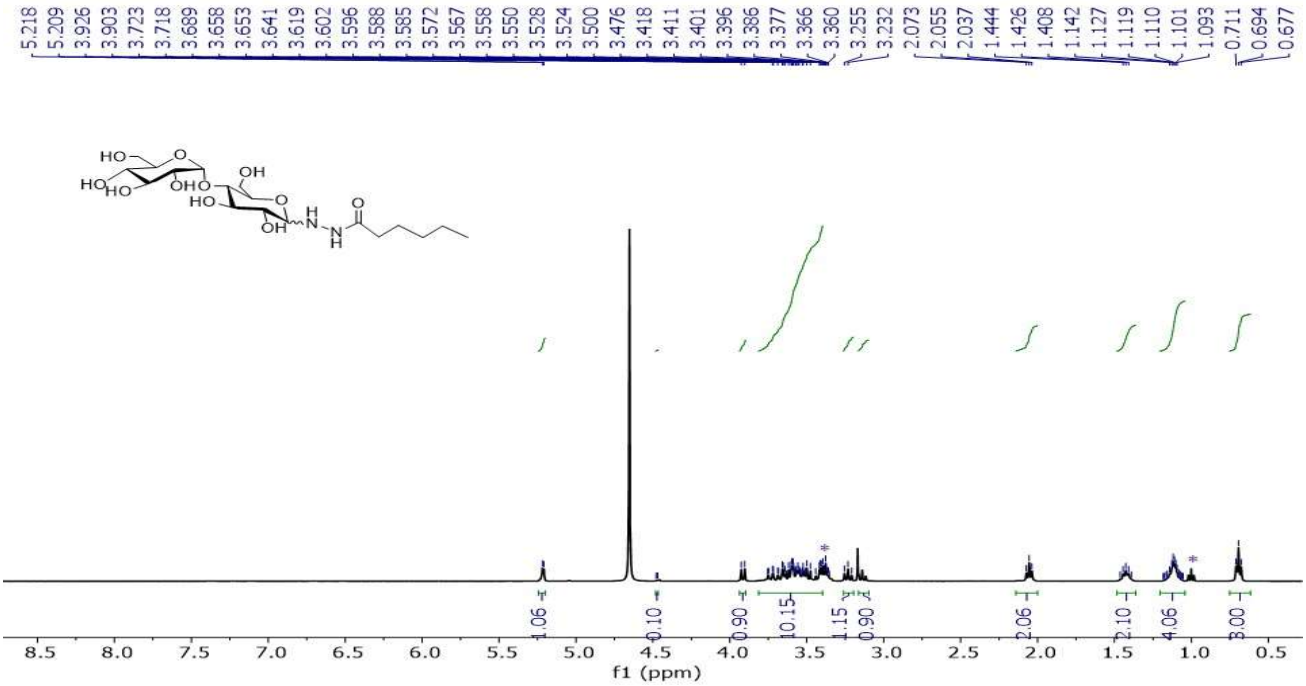

Figure S29. ^{1}H NMR spectrum of **4c** (n = 5) in D_2O. (The labeled peaks are related to the residual diethyl ether used in the last step of purification).

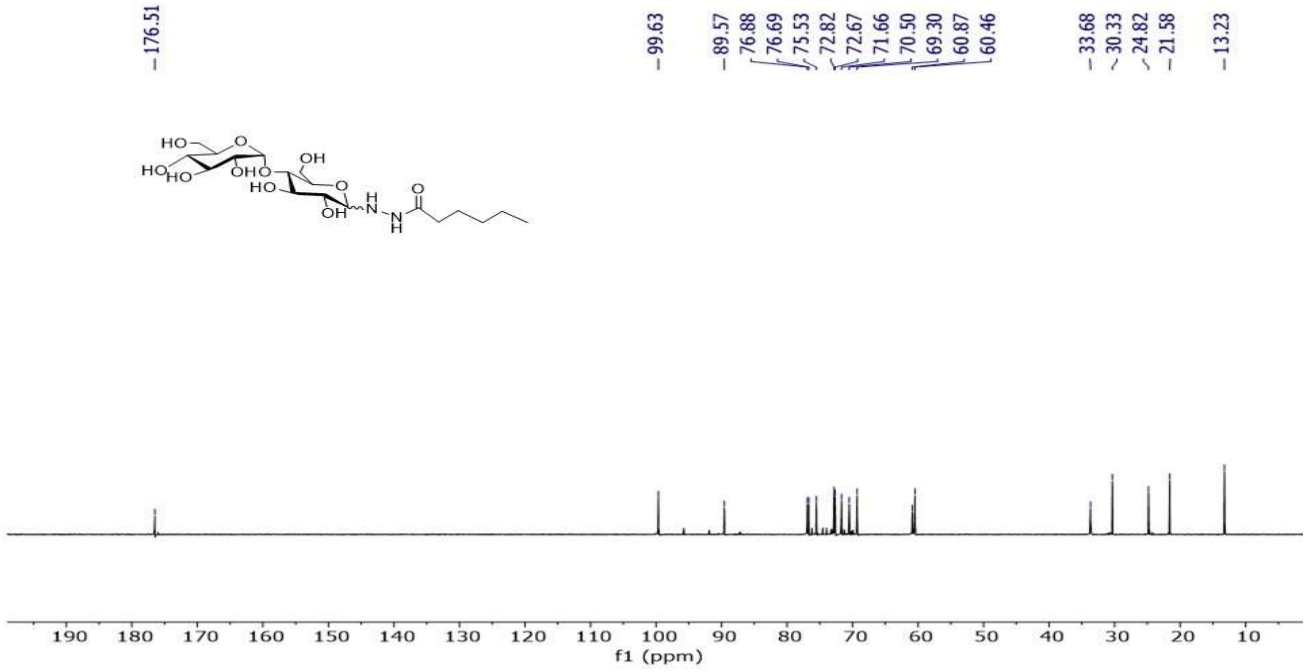

Figure S30. ^{13}C NMR spectrum of **4c** (n = 5) in D_2O.

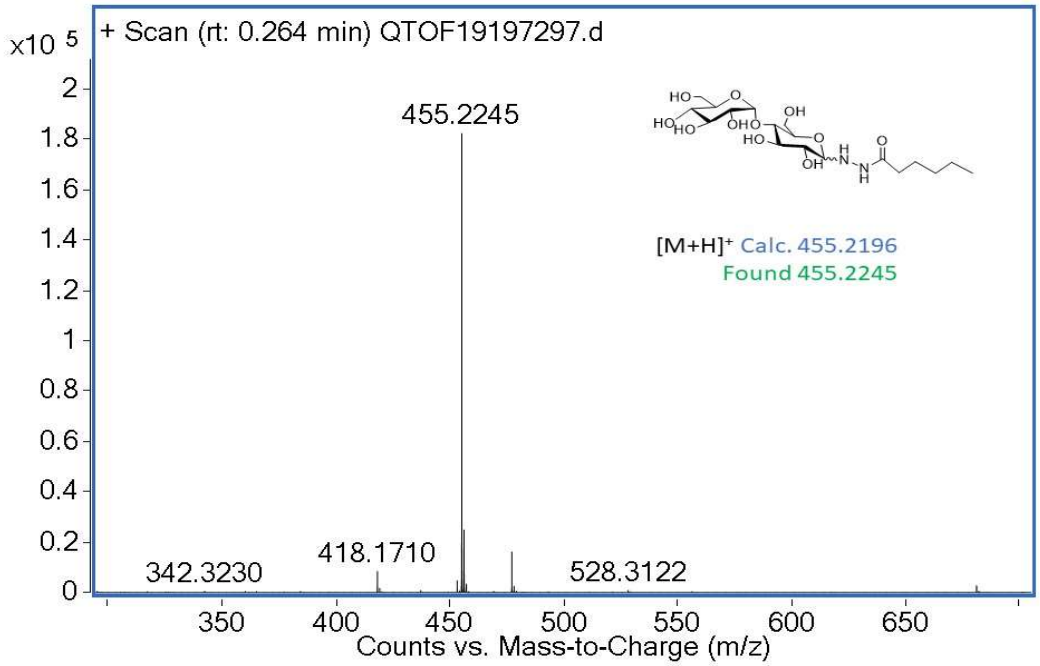

Figure S31. Mass spectrum of **4c** (n = 5).

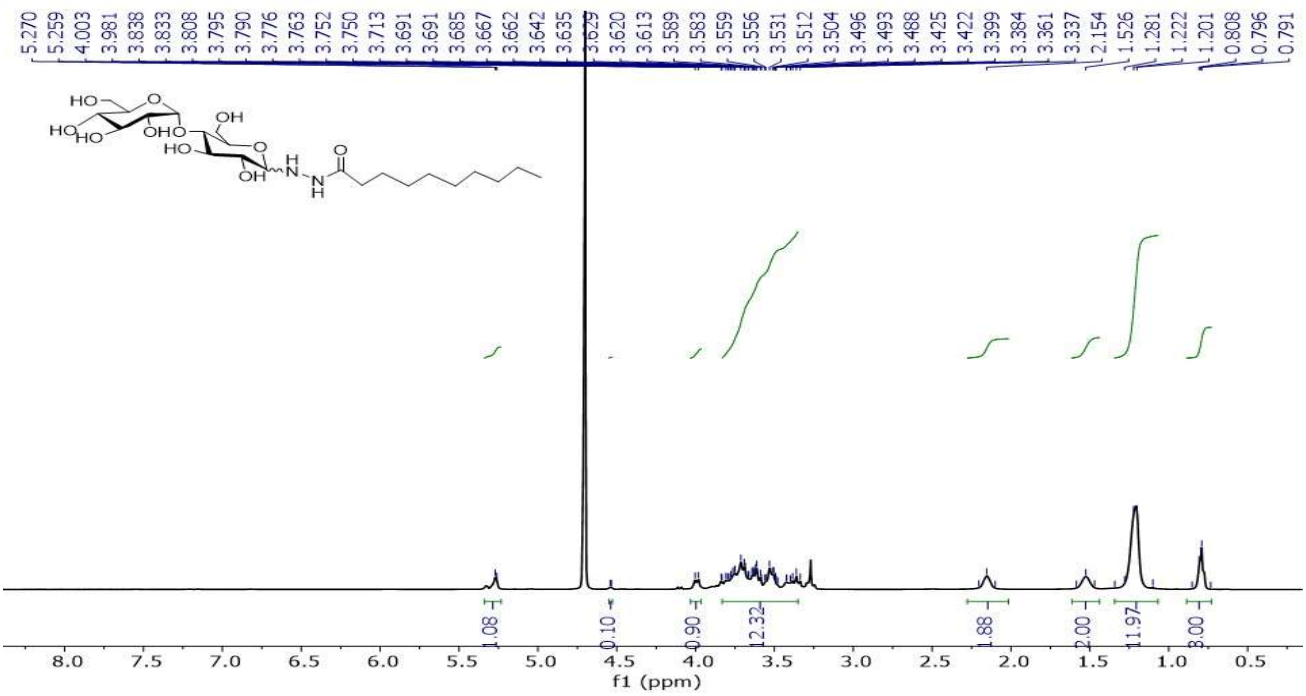

Figure S32. ^{1}H NMR spectrum of **4c** (n = 9) in D_2O.

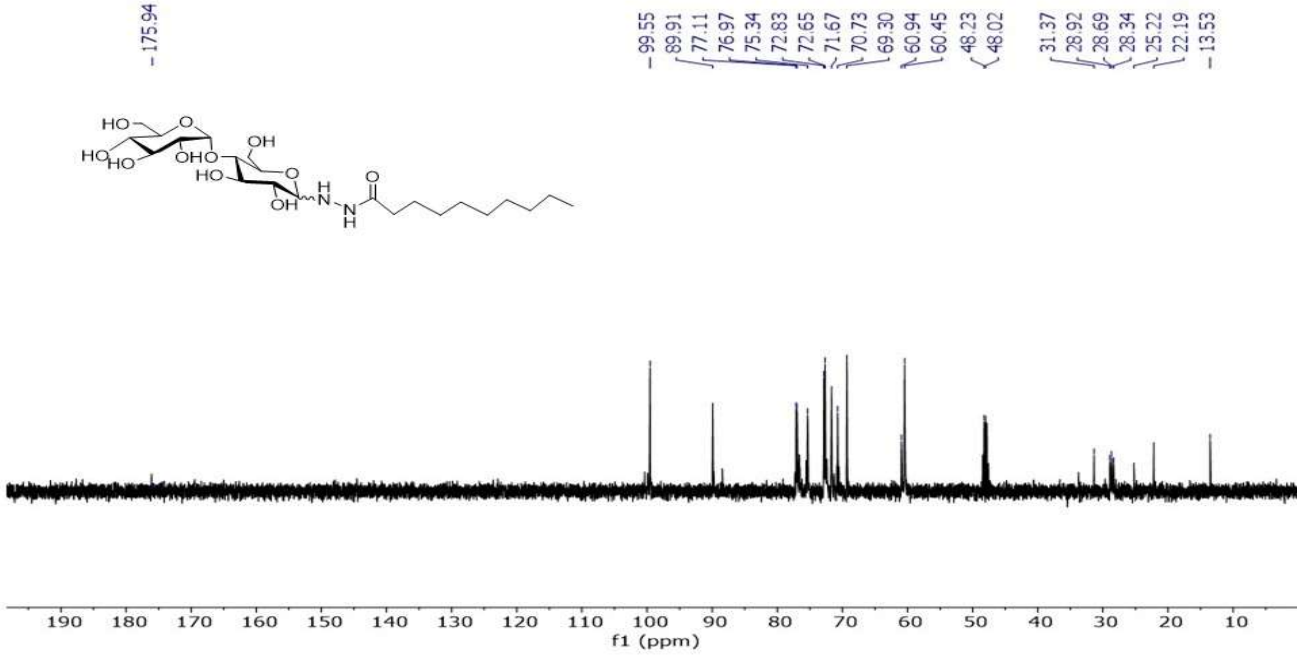

Figure S33. ^{13}C NMR spectrum of **4c** (n = 9) in D_2O.

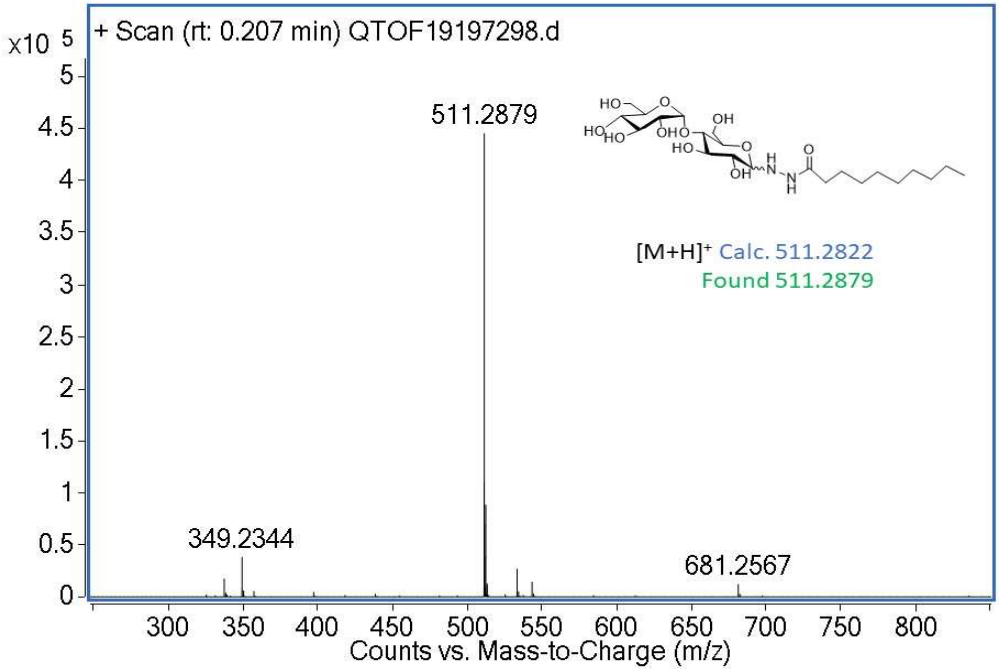

Figure S34. Mass spectrum of **4c** (n = 9).

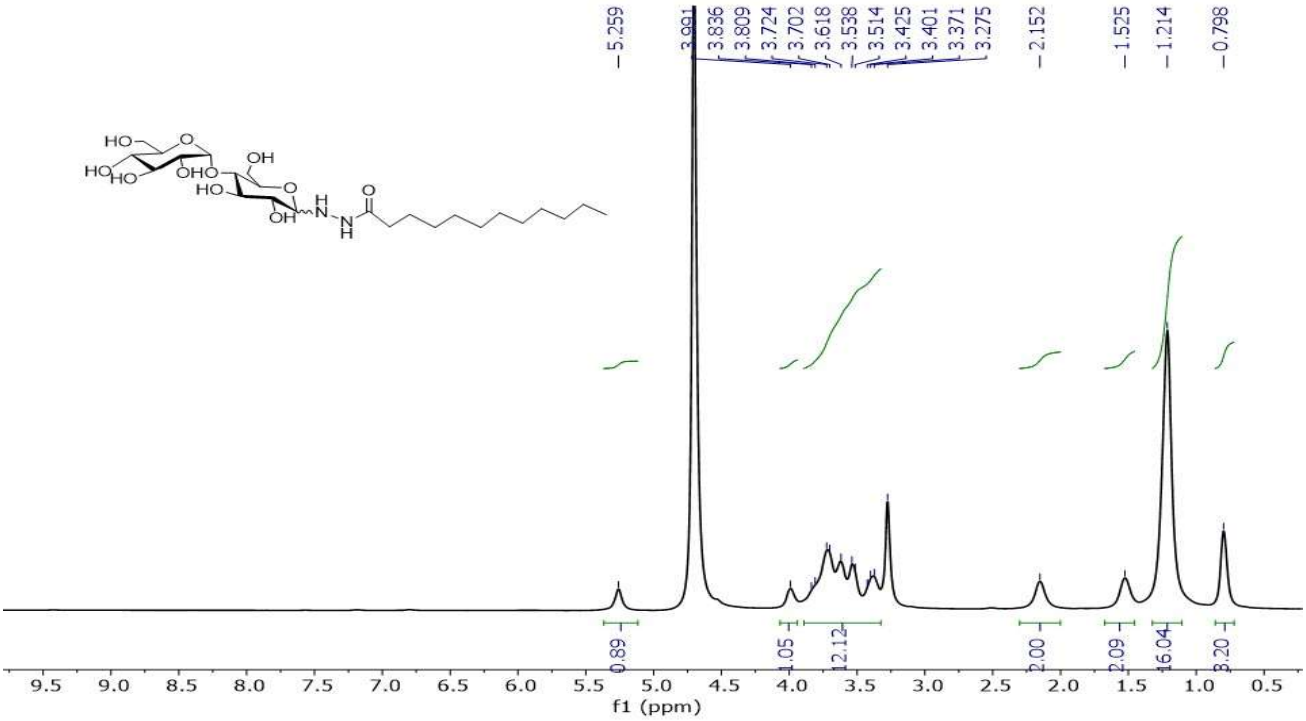

Figure S35. ^{1}H NMR spectrum of **4c** (n = 11) in D_2O.

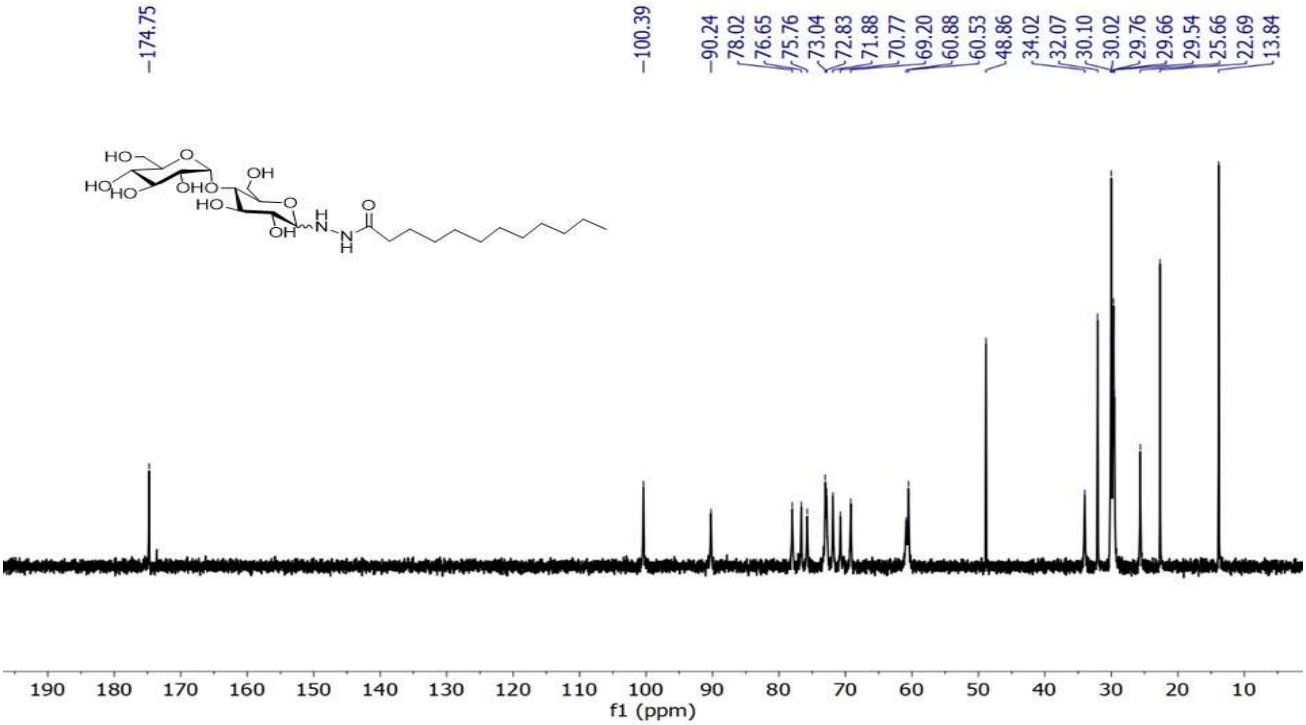

Figure S36. ^{13}C NMR spectrum of **4c** (n = 11) in D_2O.

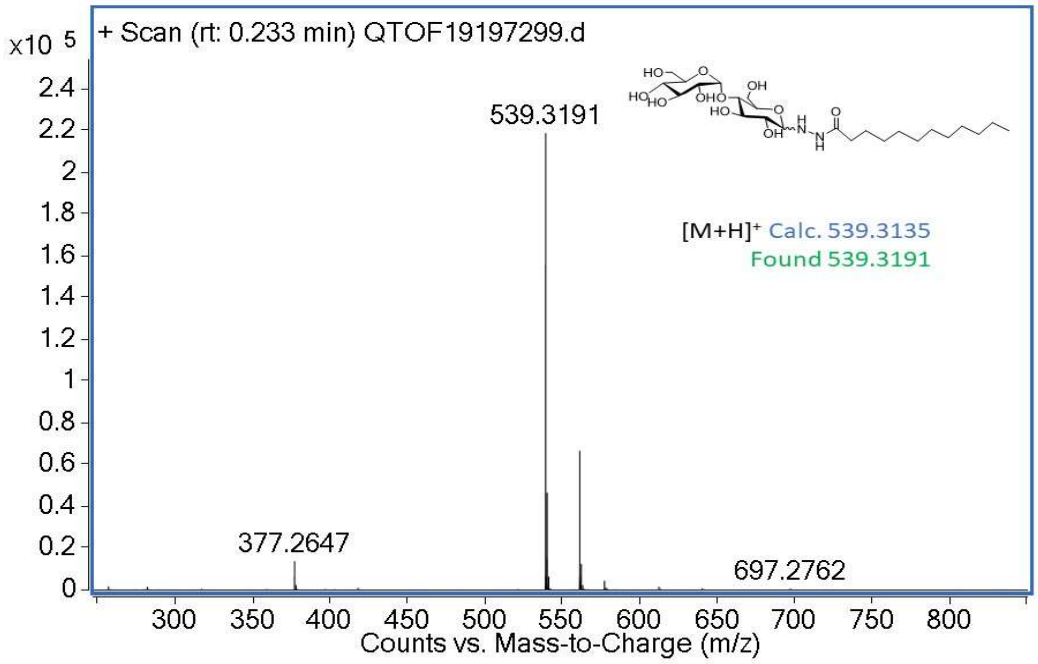

Figure S37. Mass spectrum of **4c** (n = 11).

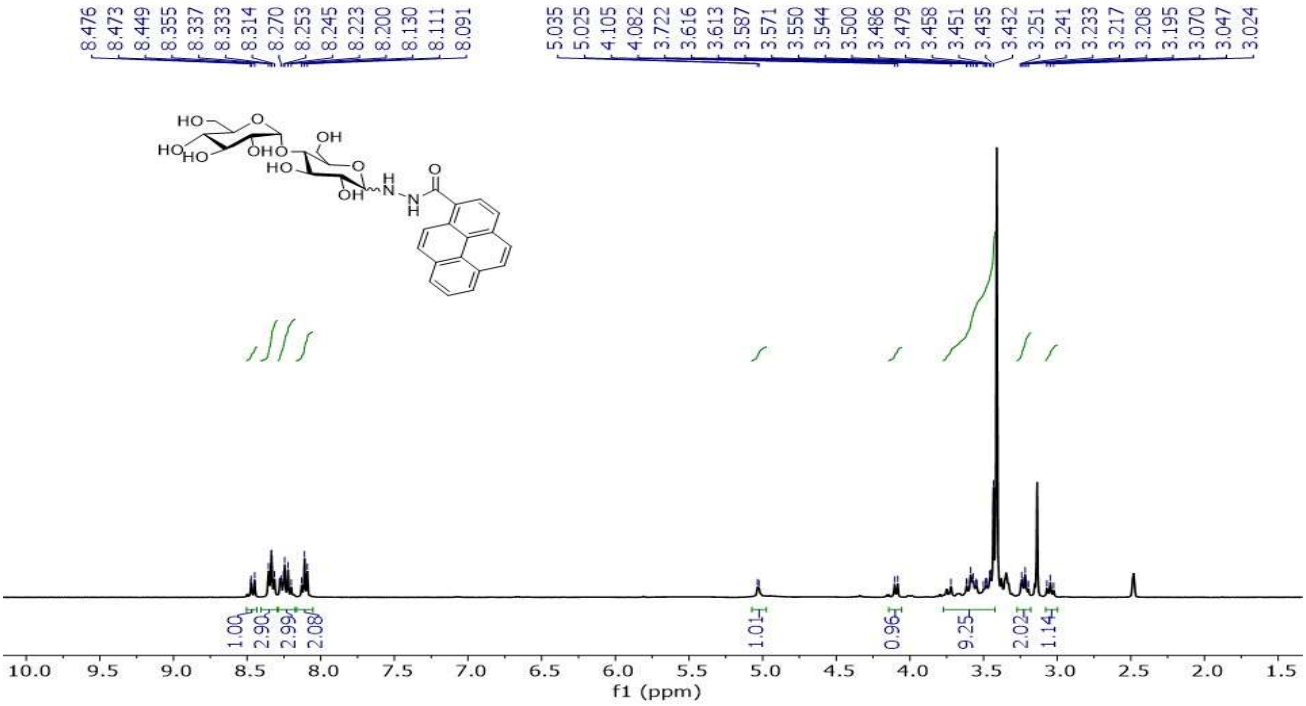

Figure S38. ^{1}H NMR spectrum of **4d** in D_2O.

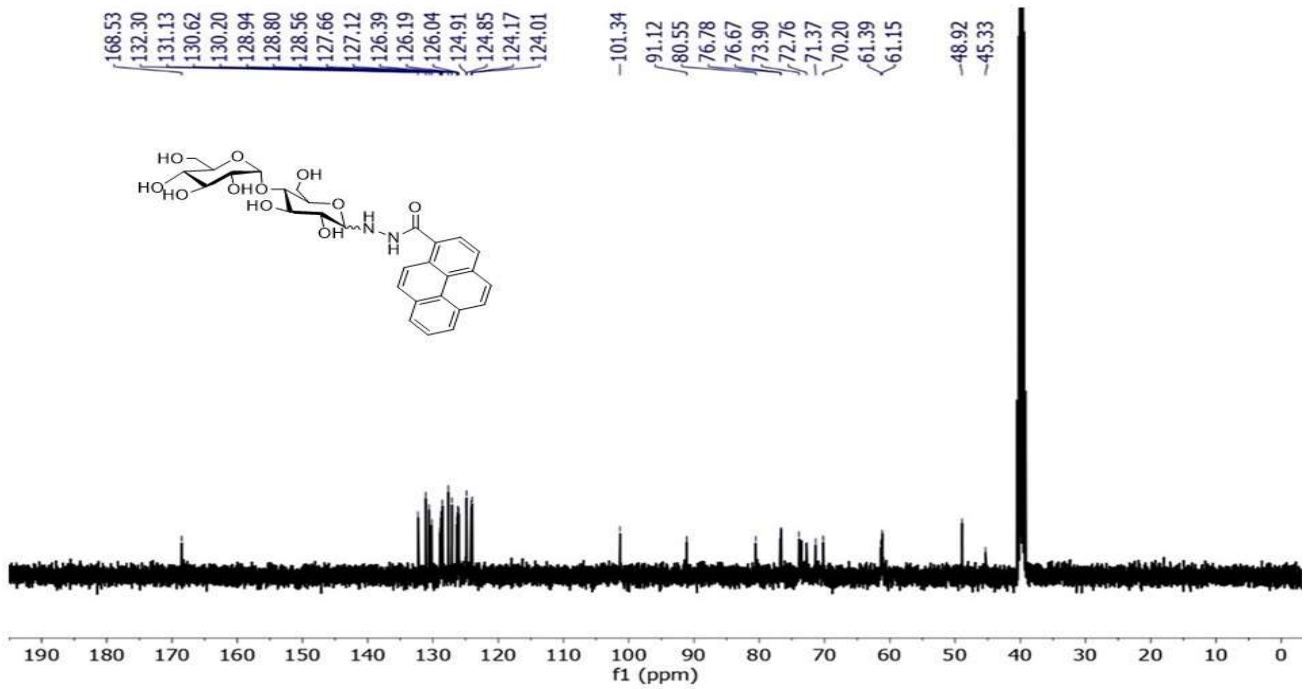

Figure S39. ^{13}C NMR spectrum of **4d** in D_2O.

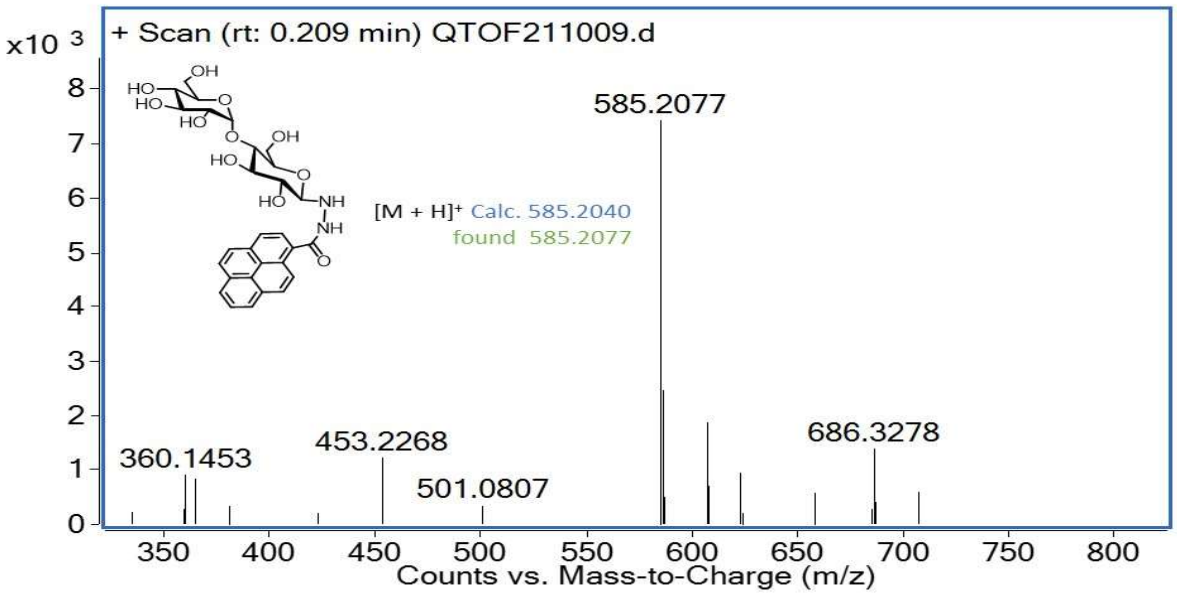

Figure S40. Mass spectrum of **4d**.

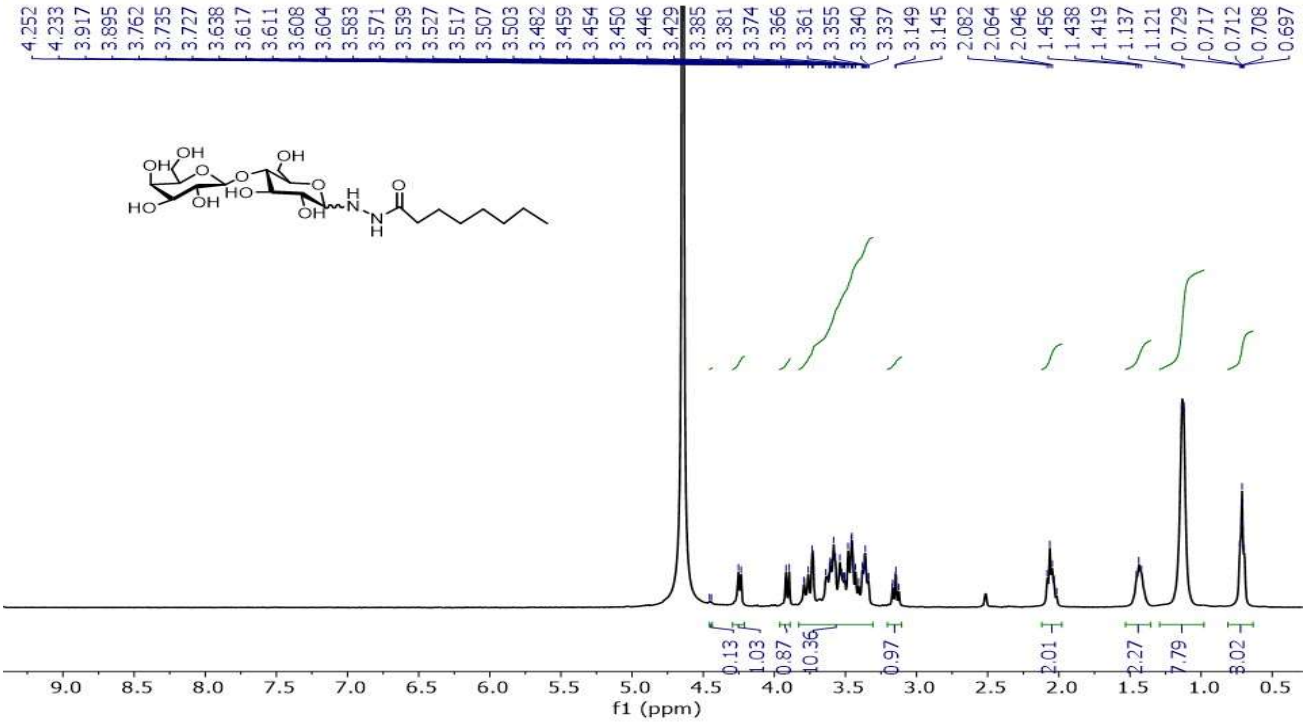

Figure S41. ^{1}H NMR spectrum of **11** in D_2O.

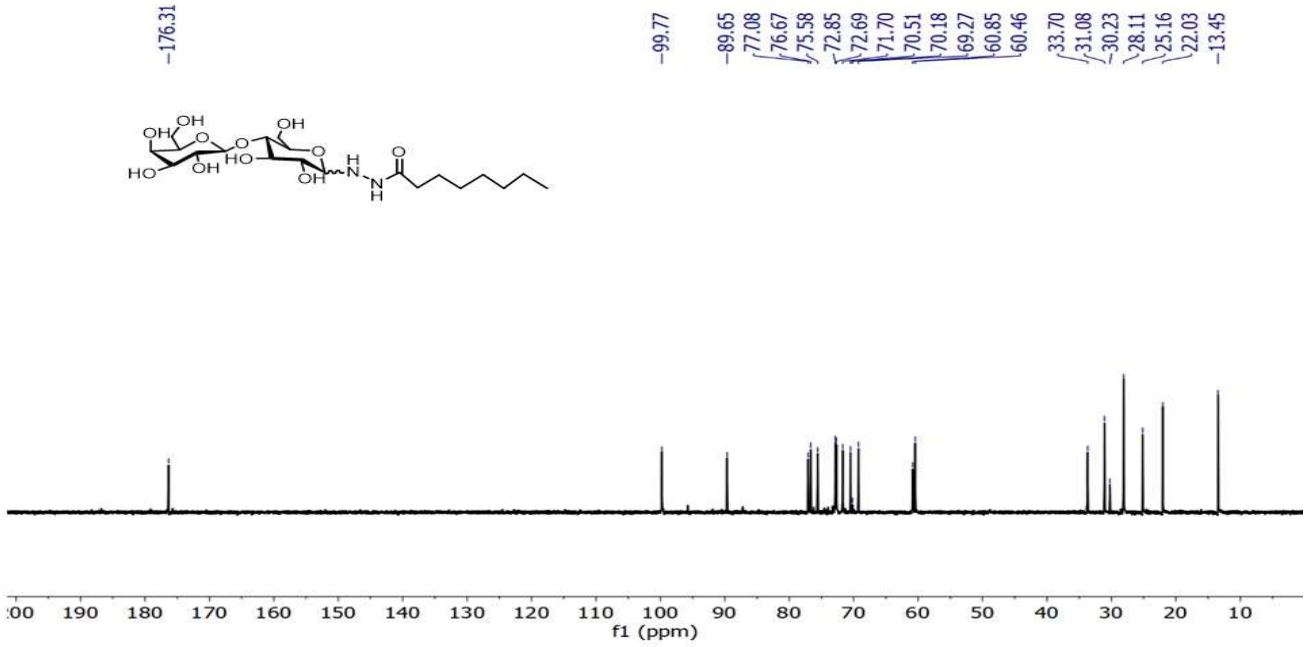

Figure S42. ^{13}C NMR spectrum of **11** in D_2O.

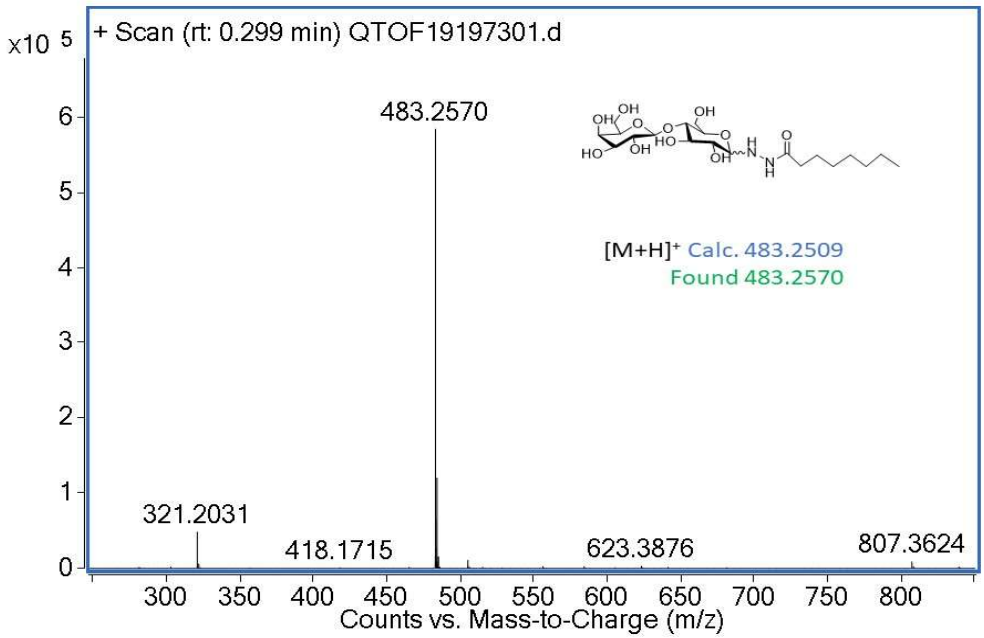

Figure S43. Mass spectrum of **11**.

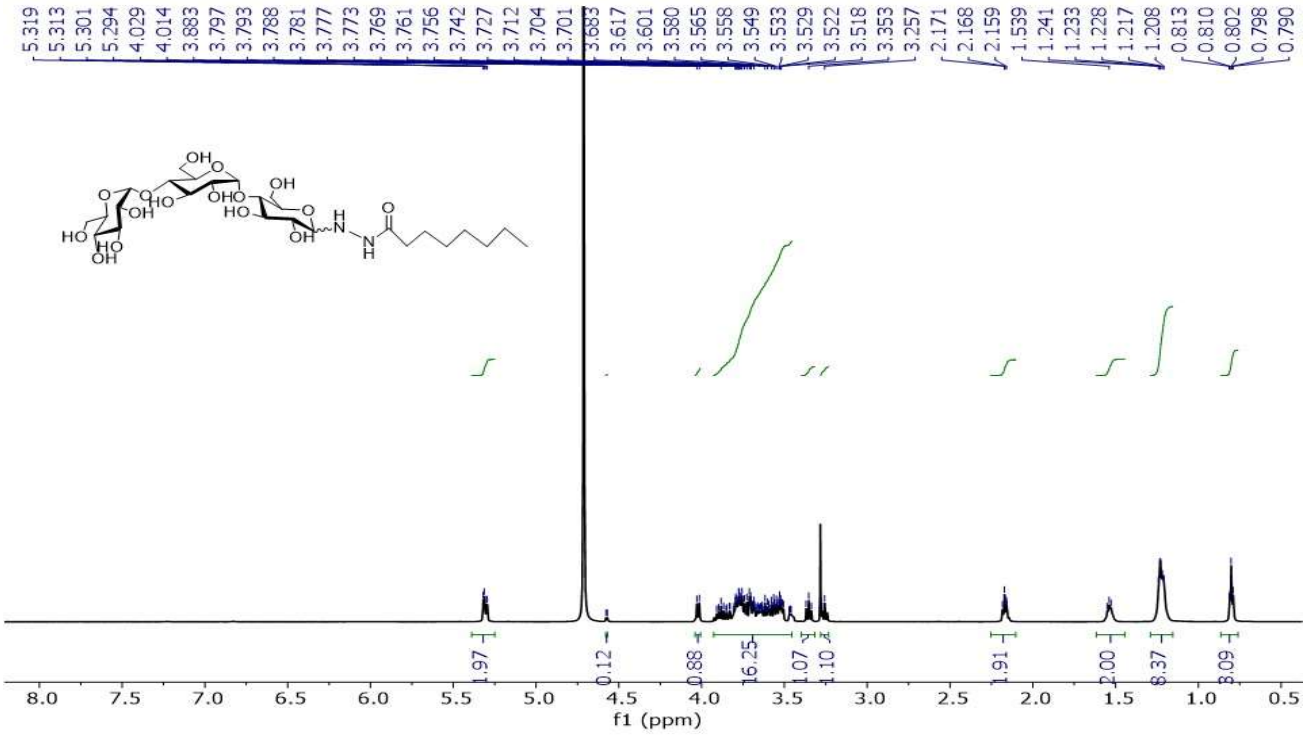

Figure S44. ^{1}H NMR spectrum of **12** in D_2O.

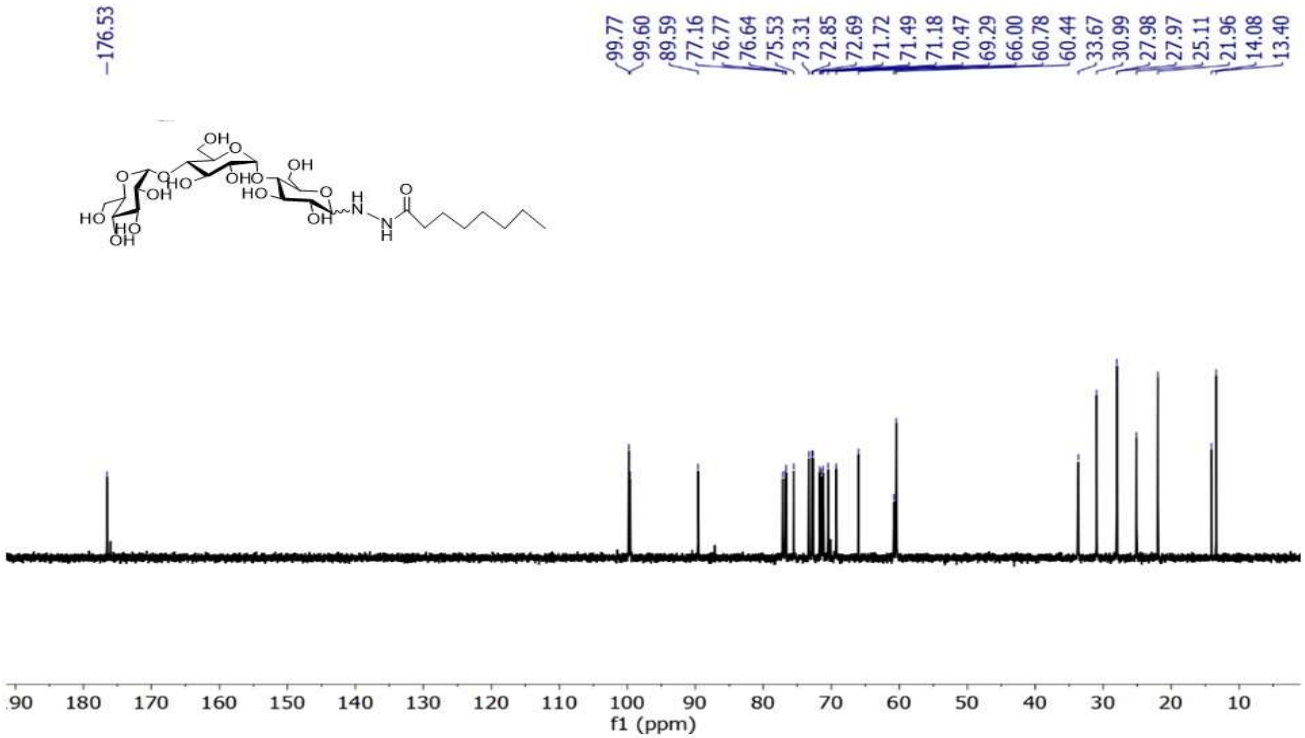

Figure S45. ^{13}C NMR spectrum of **12** in D_2O.

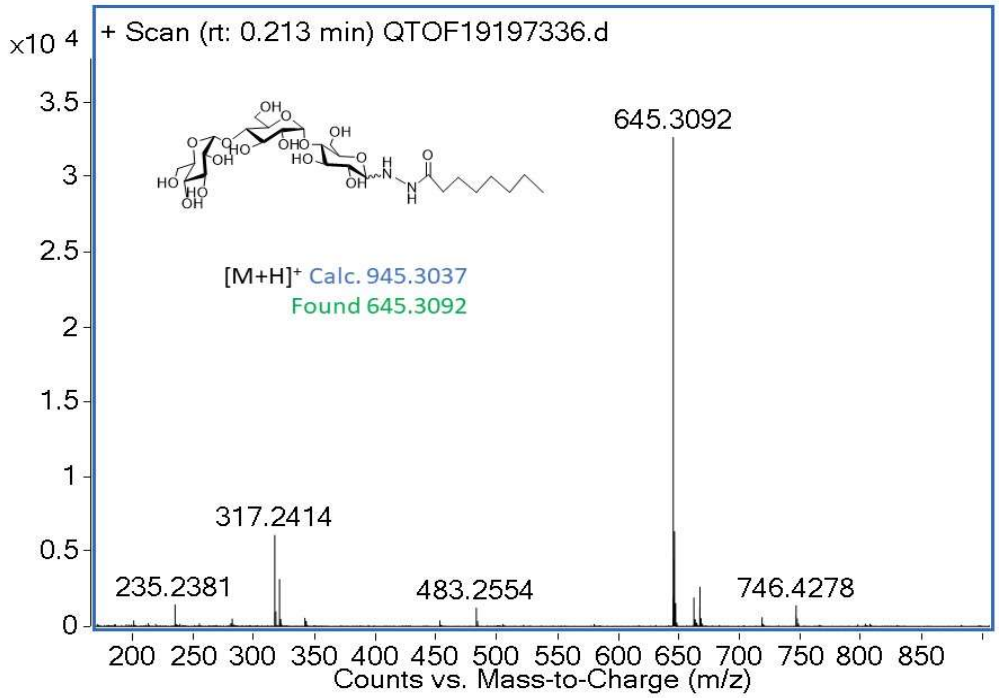

Figure S46. Mass spectrum of **12**.

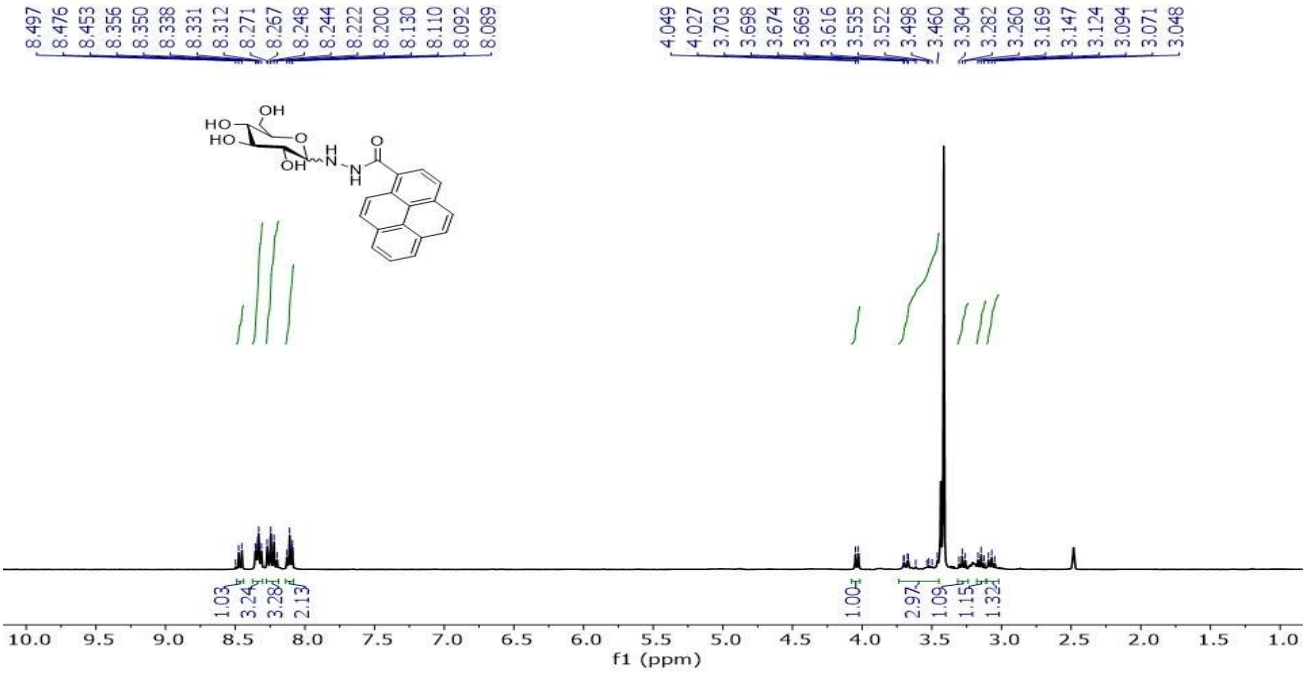

Figure S47. ^{1}H NMR spectrum of **15** in DMSO-*d6*.

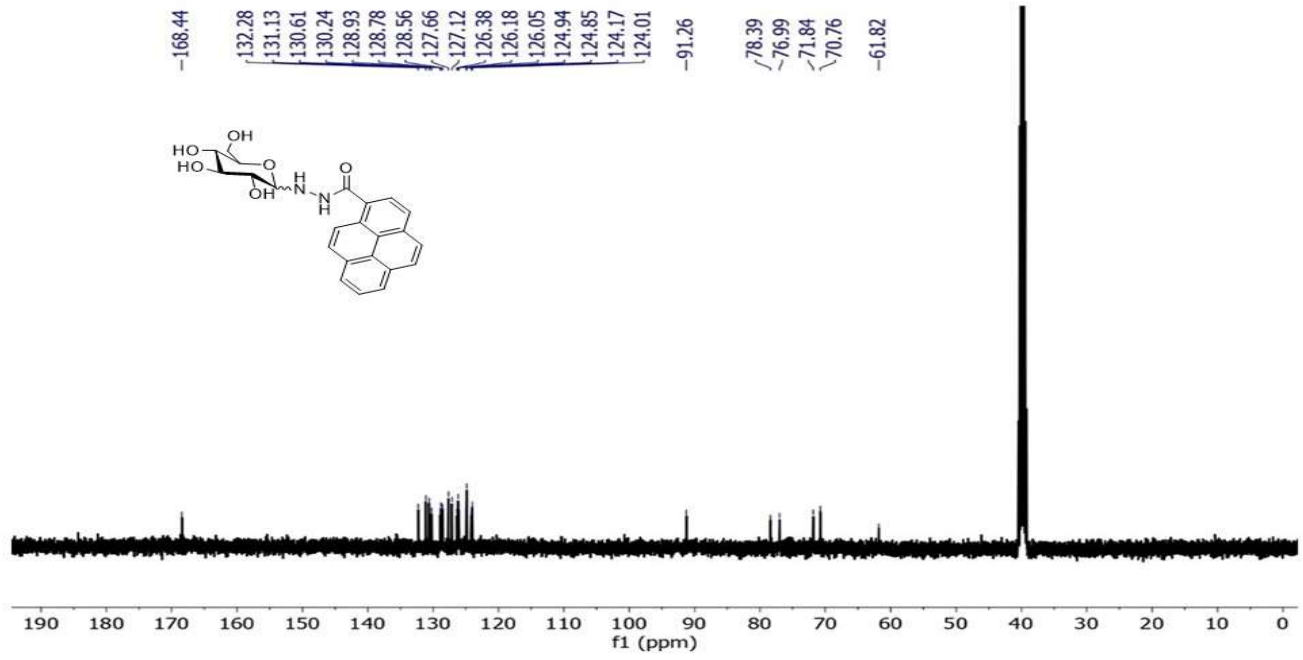

Figure S48. ^{13}C NMR spectrum of **15** in DMSO-*d6*.

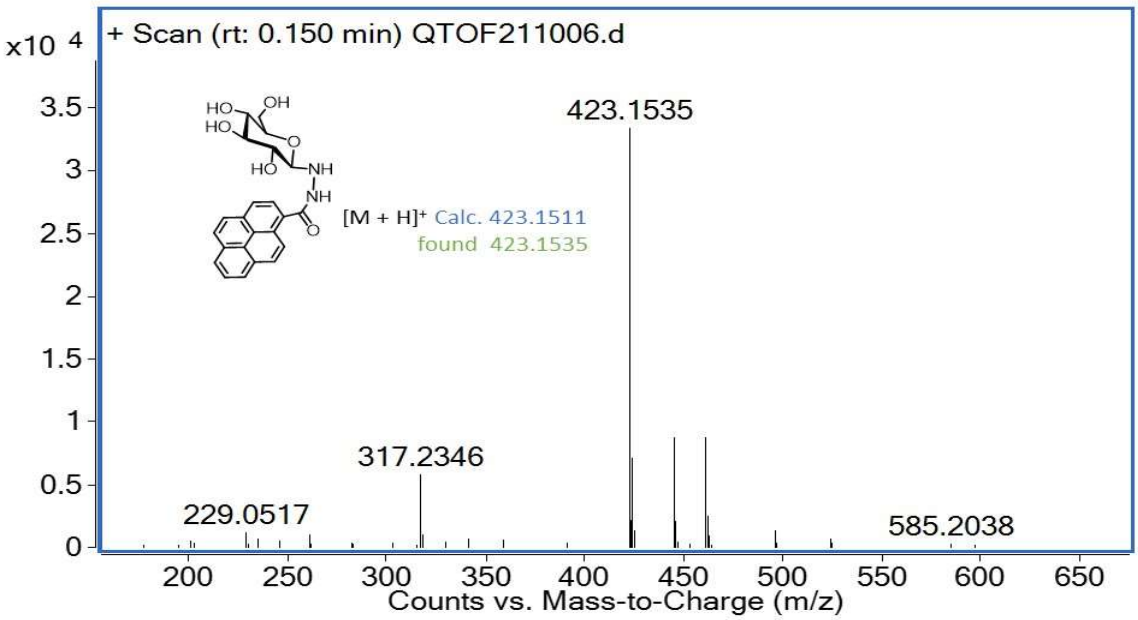

Figure S49. Mass spectrum of **15**.